# CHAPTER 25

# IGNITION OF DUST PARTICLES

**Seung Wook Baek**

Korea Advanced Institute of Science and Technology
Department of Aerospace Engineering
Seoul, Korea

## CONTENTS



## INTRODUCTION

In the investigation of the ignition of dust particles, one of the main objectives has been to find the detailed structure of detonation and explosion phenomena. Accidents are often caused due to dust, e.g., by grain dust in grain elevators or coal dust in coal mines.

Dusts are produced in many industrial processes. They may be ignited by various ignition sources and lead to flame propagation, which disperses the dust by the expansion of the burned gases. The cloud ahead of the flame is then caused to move in the direction of flame propagation and turbulence is generated. Simultaneously, the fresh mixture is heated by both heat conduction and radiation from the flame front. It may finally lead to detonation and explosion. The energy required for initiation and propagation of detonation in tubes of finite diameter depends on the structure of the reaction zone and, especially, upon the length of the induction zone. The length of the induction zone in dust detonations can be determined by measuring the ignition delay of a small cloud of dust particles behind incident shock waves.

On the other hand, the fluidized bed combustion has become a very important practical development in combustion technology. Its remarkable success has resulted from the ability of fluidized beds to burn coals of low quality. For the design and operation of the fluidized

bed combustor the ignition of solid fuel is one of the important phenomena involved. The lowest bed temperature should be known for the start-up and efficient control of the fluidized bed combustor.

Furthermore, by measuring ignition delays of various materials, their sensitivities to ignition can be assessed and compared. From this viewpoint, the experimental and theoretical information on the ignition of dust particles are presented in the following.

## EXPERIMENTS

### Introductory Remarks

Ignition delay times of various dusts have been measured by researchers using shock tubes [1–6] and fluidized bed combustors [41]. Experimentally, the definition of ignition can be specified by measuring the intensity of carbon dioxide emission, as was done in Reference [7], or the intensity of light emission as in [1, 4–6], and assigning some arbitrary level as a reference.

### Ignition Modes

There are two ignition modes: heterogeneous and gaseous ignition. Which ignition mode is more likely to occur is strongly dependent on the heating rate of solid particles. Therefore the Biot number, which is the ratio of surface temperature gradient in a solid particle to that in the gas, plays a significant role in determining the ignition mode. For metal particle ignition, the Biot number is so small that a uniform temperature distribution inside the particle may be assumed.

However, in particles such as coal and oats, the Biot number is of order unity where particles are exposed to the forced convective heating by hot gases flowing behind a shock wave. In this case, the temperature distribution inside the particle plays an important role. In addition, if the strong convective heating causes a very short ignition delay time, in which the effects of devolatilization are negligible, the solid phase type of ignition might prevail. But in conditions where the heating rate is low, for example, in the stagnant hot gases created by a reflected shock wave [1, 6, 8–9], the assumption of a uniform temperature distribution might be acceptable. This is because the rate of heat transfer to the inside of the body from the surface in contact with the hot gases is comparable to the heating rate of the surface by the hot gases. Consequently there is enough time for substantial amounts of volatile gases to be given off by the particle, and the ignition mode may then be of the gaseous type. The gas-phase ignition of coal in oxygen was observed in reflected shock experiments [10].

In [11], the devolatilization effect was found to be negligible in a shock wave ignition study and this was proven by experimentally measuring and comparing the ignition delays of coal, graphite, and char under the shock tube conditions. Thus the heterogeneous ignition mode was proposed in incident shock experiments.

### Ignition Delays

#### *Incident Shock Wave Ignition*

In [4], ignition delay times behind incident shock waves were measured in pure oxygen for the various materials as listed in Table 1. The ignition delay time was defined as the time interval between the interaction with the dust cloud and the appearance of light. Figure 1 shows a schematic diagram of the experimental set-up. A small cloud of dust particles is

**Table 1**
**Dusts Investigated**

| Substance | Particle-Size Range ($\mu$m) |
|---|---|
| Coal (Pittsburgh Seam) | 53–74 |
| Graphite | 53–74 |
| Oats | 53–74 |
| Diamond* | 4–6 |
| RDX-E | 2 (mean diameter) |
| RDX-E* | 2 (mean diameter) |
| RDX-A* | 37 (mean diameter) |

* *Implies addition of 10% Cabosil by weight.*
*Reprinted from [4] with permission of the American Institute of Aeronautics and Astronautics.*

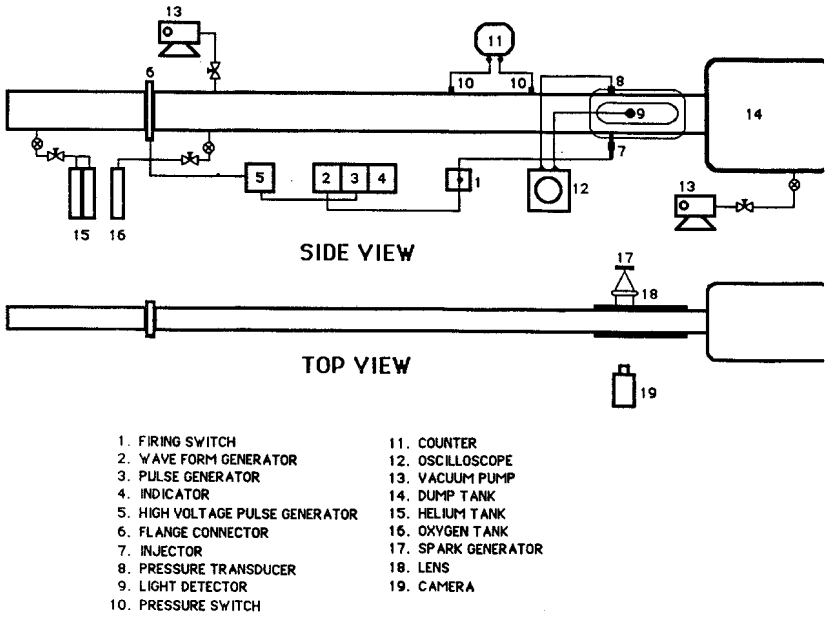


**Figure 1.** Schematic of experimental setup for incident shock wave ignition.

injected into the test section just before the arrival of the shock wave. Two different types of injectors were used: an inertial injector, which is operated by inertial force as shown in Figure 2; and a pneumatic injector, as shown in Figure 3, whose driving force is the pressure difference between the inside and outside of the shock tube.

Typical clouds formed by the two different injectors are illustrated in Figures 4 and 5. When dust was loaded into the three holes of the inertial injector tip, which was installed on the top of the shock tube, a small compressive force was applied. Therefore, after the dust

was introduced into the test section by the inertial force, both large and small agglomerations were observed in the cloud as shown in Figure 4. The pneumatic injector, on the other hand, was installed at the bottom of the shock tube with the dust dropped freely on several screens inside the injector tip. As shown in Figure 5, the dust was injected in a well-dispersed pattern by the air flow, which was induced by the movement of a piston. For the detailed experimental procedure, see [4].

In Figure 6, the experimental results for coal and graphite are plotted on a logarithmic scale for both injectors versus the inverse of post-shock gas static temperature, nondimensionalized by the initial temperature, together with its corresponding incident shock wave Mach number. All the experimental data were obtained with pure oxygen to prevent the

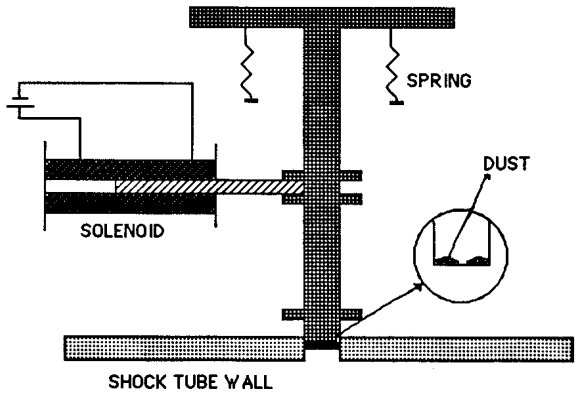


**Figure 2.** Inertial dust injector (based on [4] with permission of the American Institute of Aeronautics and Astronautics).

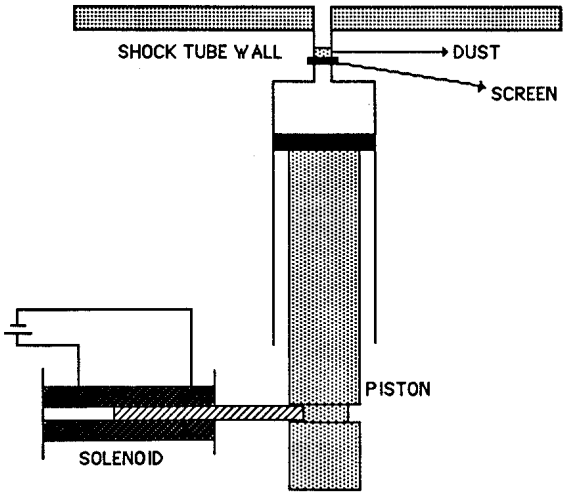


**Figure 3.** Pneumatic dust injector (based on [4] with permission of the American Institute of Aeronautics and Astronautics).

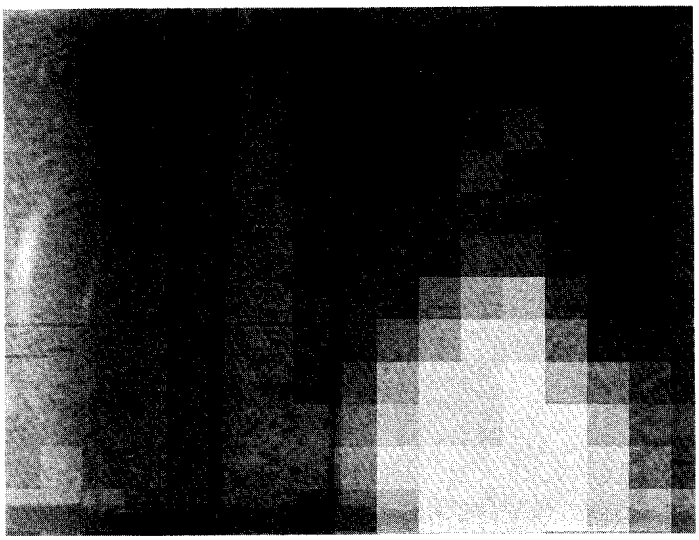

**Figure 4.** Shadowgraph of dust clouds formed by an inertial injector.

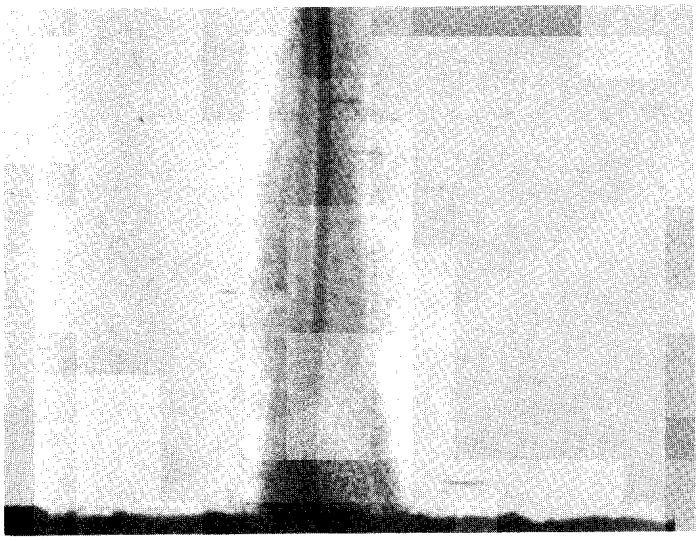

**Figure 5.** Shadowgraph of dust clouds formed by a pneumatic injector.

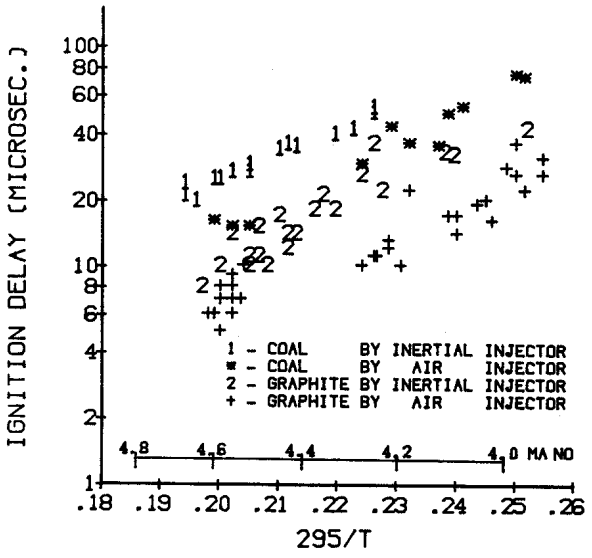


**Figure 6.** Ignition delay data for pure oxygen (reprinted from [4] with permission of the American Institute of Aeronautics and Astronautics).

whole phenomena from being controlled by the diffusion of oxygen to the particle surface. The values of the post-shock static temperature ranged from 1,160 to 1,600 K. This form of representation is typically used for systems governed by an Arrhenius rate law, and then the slope of the delay curve is proportional to the activation temperature. The data appear to lie on a straight line for the range of experiments. The temperature range above corresponds to Mach numbers ranging from 4 to 5, as indicated on the Mach number scale above the inverse temperature scale. As was expected, the ignition delay time decreased with increasing incident shock wave Mach number. Since the inertial injector produces clouds with a considerable particle agglomeration, the observed ignition delays are somewhat longer than with the pneumatic injector.

In Figure 7, the experimental data for other dusts injected by the inertial injector are displayed. Although all the delay times are below 100 $\mu$s, there is a wide discrepancy among the different materials. Oats dust has a significantly shorter delay time than coal dust, suggesting that it is also a more detonable material. Interestingly, RDX-A (mean diameter 37 $\mu$m) with Cabosil has shorter delay than RDX-E (mean diameter 2 $\mu$m) with Cabosil. This supports the observed stronger detonability of RDX-A versus RDX-E. However, it should be noted that the smaller particles would be heated and ignited faster than the larger particles from the point of view of heat transfer. The ignition delay of the very small diamond particles is comparable to that of the much larger graphite particles and is probably related to the surface properties of these two forms of carbon.

Straight lines obtained from the data using a mean square fit are shown in Figure 8. Their equivalent activation energies, which are proportional to the slope for each curve, are also indicated in the figure.

Based on [12], ignition delay times are given in Figure 9 for three different dusts: coal, milo, and Kansas City red wheat. In all cases, air has been used as an oxidizer. Three different sizes of dust were run: less than 37 $\mu$m, 37–54 $\mu$m, and 55–74 $\mu$m. As little size effect was seen on the ignition delay data, these classifications are not differentiated here. The coal

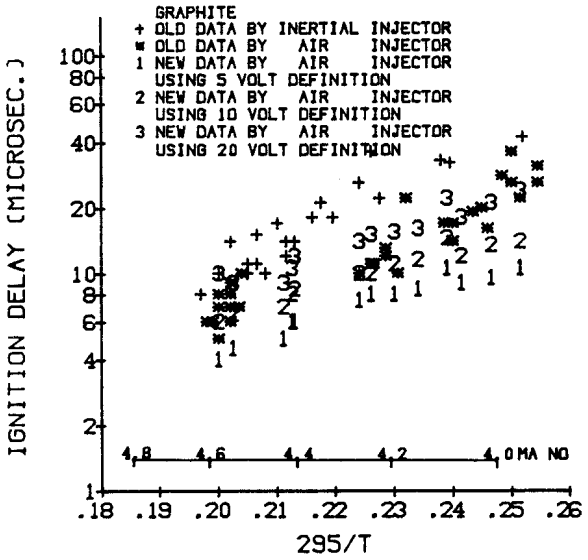


**Figure 7.** Ignition delay data for pure oxygen (reprinted from [4] with permission of the American Institute of Aeronautics and Astronautics).

dust is included in that one may recall that it is the standard of explosibility testing in the Hartman apparatus. Milo and wheat dust are seen to be more reactive than coal dust. In fact, the ignition delay times for wheat can be quite short, and indeed comparable to those for gaseous hydrocarbons. The activation energies are similar to those for gas-phase reactions. The data in Figure 10 show a comparison between two similar but chemically different substances: wheat and white wheat flour. The difference no doubt reflects the removal of certain components of the grain before the production of the flour.

In Figure 11, the longer ignition delay data obtained from the vertical shock tube are combined with the data from the horizontal tube. In the former case, the dust used was simply smaller than 74 $\mu$m, while in the latter case it was between 53 and 74 $\mu$m. For the case of vertical tube, dust is fed into the tube at a controlled rate by a feeder in order to produce a known dust concentration along the entire length of the tube. When the mixture has been established, the ball valve is closed to protect the feeder, and a combustion process is initiated in the hydrogen/oxygen mixture in the initiator tube.

The data collected using the two different systems are in good agreement for corn, soybean, and Hutchinson hard red winter wheat. Wheat again is seen to be the most reactive substance.

A comparison is made in Figure 12 between the two different types of wheat dust in the same size range and for oats dust having a slightly smaller size. Not only do the two different "identical" wheats show different ignition delay times, but they have different activation energies. The oats data show that it, along with wheat, is one of the more reactive dusts. Figure 13 represents the ignition data on pet food dust, which is no more reactive than coal dust.

From Figures 9 through 13, it can be summarized that

1. The ignition process is adequately described by an Arrhenius rate law.
2. For dust sizes less than 74 $\mu$m, there is little size effect.

3. Significant differences exist between different grain dusts.
4. Agricultural dusts are more readily ignitable than coal dust.

Reference [3] reported experimental data on ignition of 17-$\mu$m-diameter magnesium particles behind the incident shock wave. These data are reproduced in Figure 14.

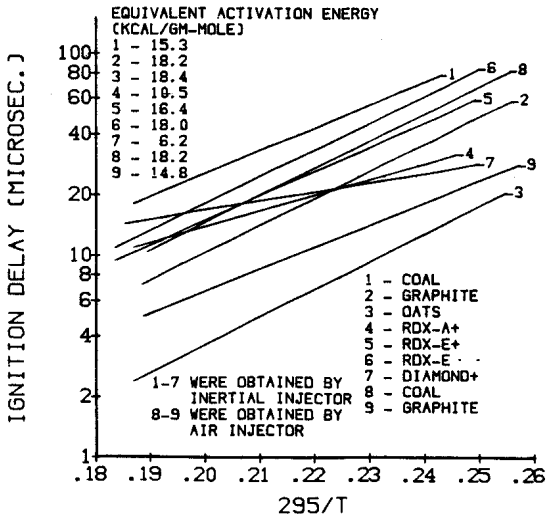


**Figure 8.** Linear curves based on mean square fit to experimental ignition delay data.

*Reflected Shock Wave Ignition*

In the foregoing section, the ignition data of dust particles behind incident moving shock waves were presented. In that case, the dominant mode of heat transfer that contributes to the particle ignition is the convective heat transfer by the hot gas flow around the particle neglecting radiative heat transfer. The plausible ignition mode for coal under incident shock wave conditions was found to be the surface ignition as assisted by [4, 11], because the volatile production by thermal decomposition of coal requires longer than the measured ignition delays according to [13].

To investigate the ignition of dust particles in the absence of forced flow around the particle, the reflected shock waves were employed by [1, 8–9] for the case of coal. As in Figure 15, [l] reported the measured ignition delay of Pittsburgh seam coal as a function of the temperature behind a reflected shock in air. Ignition delay, for this study, is defined as the time interval between the instant the incident shock disperses the particles and the instant the photomultiplier tube detects visible radiation. It was carried out under the conditions of 1–1.5 atm pressure behind the reflected shock using two particle sizes, 41 $\mu$m and 19 $\mu$m. For the ranges of gas pressure and particle size investigated, the ignition delay decreases as the gas temperature increases. The plot suggests the existence of minimum gas temperature for ignition as the delay curves become asymptotic with the delay-time axis. It appears that 41-$\mu$m coal has longer ignition delays than 19-$\mu$m coal, the difference being larger for lower gas temperatures.

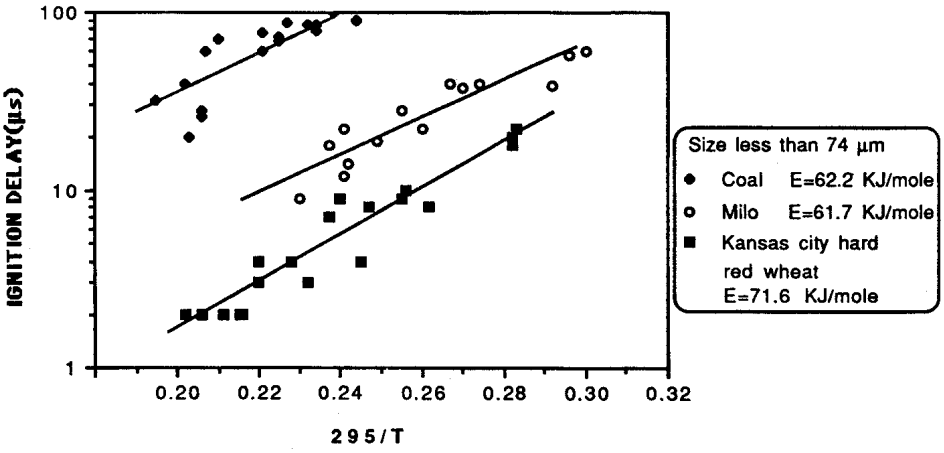


**Figure 9.** Ignition delay data for air (based on [12]).

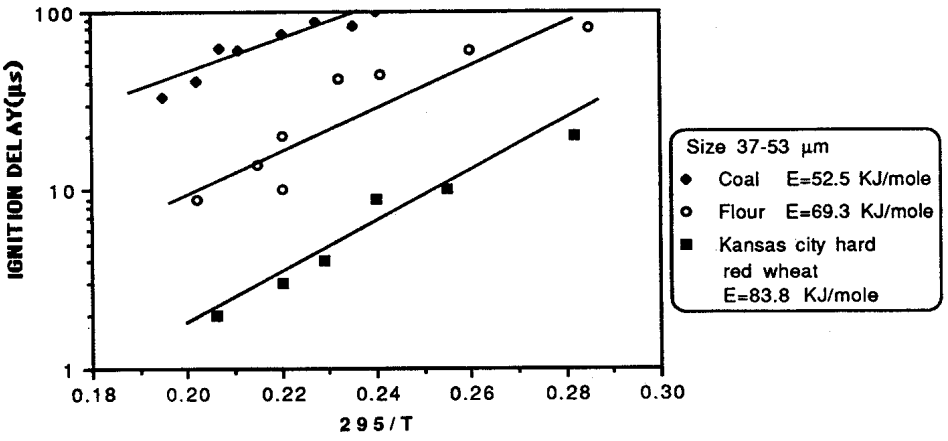


**Figure 10.** Ignition delay data for air (based on [12]).

On scanning the samples, it was also observed in [1] that unheated coal generally tended to have a sharp, angular external surface, the size of the particles varying sufficiently. When heated to various temperatures, one notices that the angular external surface gets rounded and there appears to be an increase in the overall sizes.

Reference [8] has employed two bituminous coals, an Illinois number 6 and a Pittsburgh seam, in their single-pulse shock study. The indication of ignition was afforded by both line emission from the incandescent coal particles and laser extinction. With burnout, the particle volume fraction decreased, and the resulting change in laser transmission was interpreted as the particle ignition point. The general behavior of the ignition delay of the coal samples

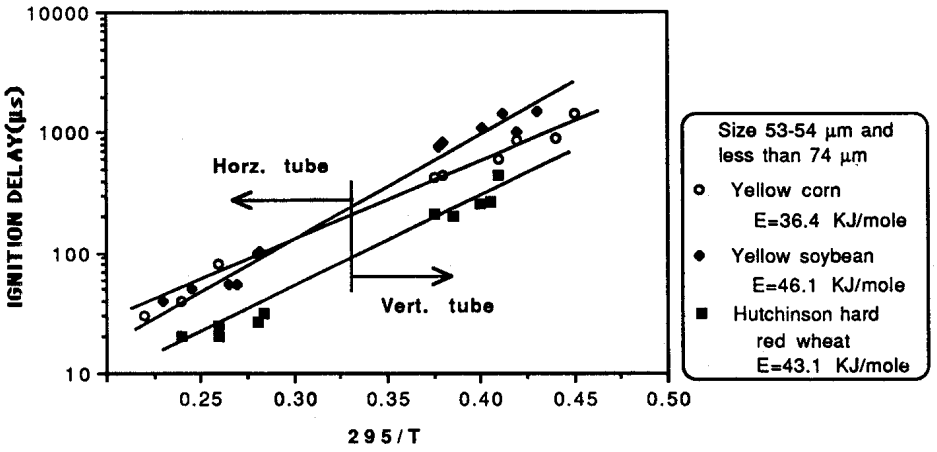


**Figure 11.** Ignition delay data for air (based on [12]).

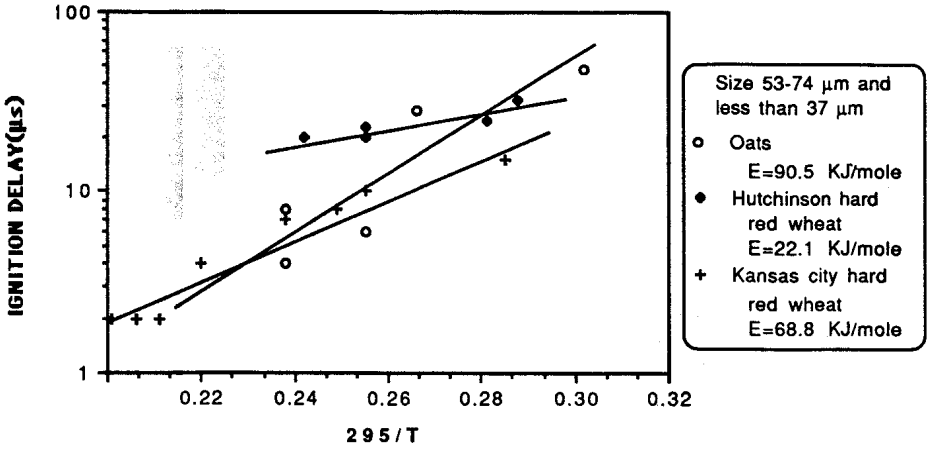


**Figure 12.** Ignition delay data for air (based on [12]).

versus gas temperature is demonstrated in Figure 16. The experimentally determined activation energies for the Arrhenius-type ignition delays are 20,800 cal/mole for Illinois number 6, 30,500 cal/mole for Pittsburgh seam (3.3 μm), and 43,600 cal/mole for Pittsburgh seam (14.9 μm). The effect of particle size was demonstrated by comparison of the delays of the two-size-classified Pittsburgh seam samples. As intuitively expected from the heat-up consideration, the larger coal did demonstrate the longer delay. The surprising result of the ignition delay measurements was the effect of coal type. The Illinois and the Pittsburgh seam (3.3 μm), samples with similar ASTM volatile matter content and with comparable size distributions, had markedly different ignition delays. In fact, the slightly larger Illinois coal demonstrated a shorter delay at any temperature, and only during the highest temperature runs did the two samples exhibit the same delay.

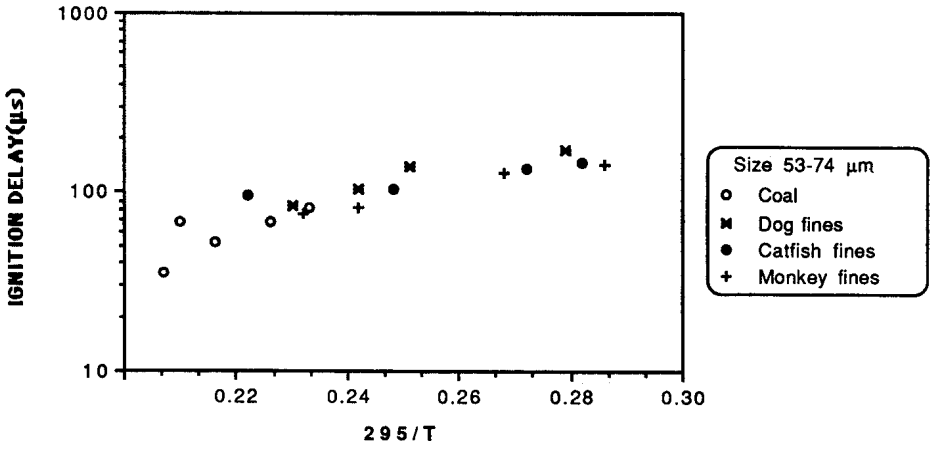


**Figure 13.** Ignition delay data for air (based on [12]).

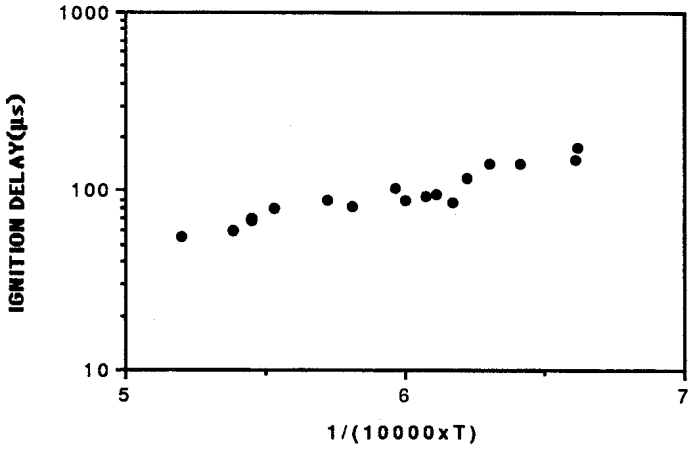


**Figure 14.** Ignition delay data of magnesium particles with diameter 17 μm (based on [3] with permission of the American Institute of Aeronautics and Astronautics).

In [8], the surface oxidation rates were determined by analysis of the rate of decrease of the laser line extinction. The behavior of these measurements as a function of gas temperature is shown in Figure 17 for three samples. It must be noted that measurements of the large Pittsburgh seam sample had to be corrected for diffusion rates similar to the technique described in [14]. It was found that the surface oxidation rate generally approximated an Arrhenius behavior with the initial gas temperature. The Illinois coal had a much faster surface reaction rate than the Pittsburgh coal by a factor of 1.5 to 3, depending on the gas temperature.

In [9], ignition delay times of coal particles were determined by a shock-tube technique that permitted test times of up to 40 ms. The ignition of particles, of high volatile Utah coal was determined by detection of visible radiation from a flame region around the particles and

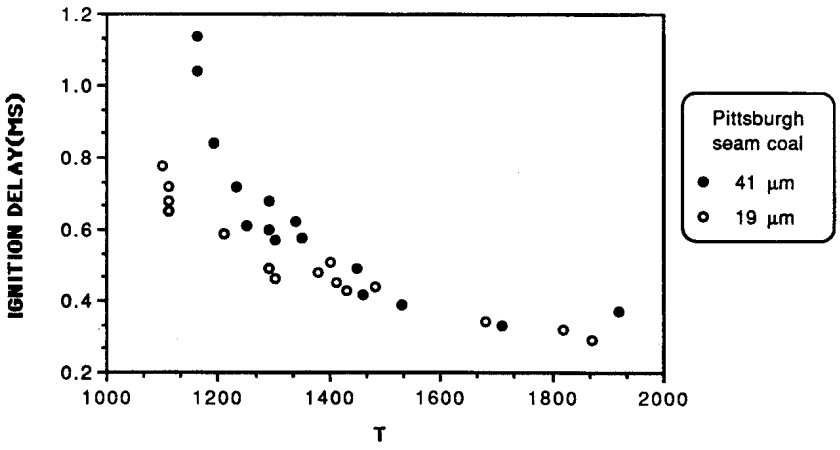


**Figure 15.** Ignition delay as a function of the temperature behind a reflected shock in air (based on [1] with permission of Gordon and Breach Science Publishers Inc.).

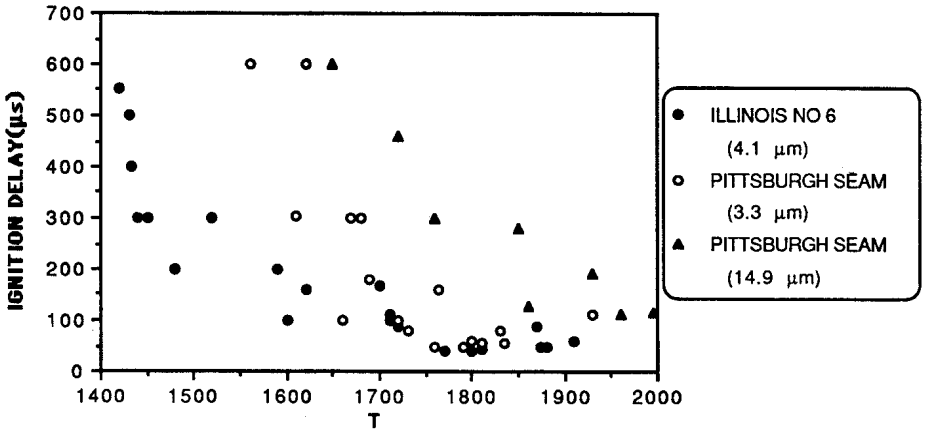


**Figure 16.** Ignition delay as a function of initial reflected shock gas temperature. $P_O$ = 1.6 atm, $P_N$ = 6.4 atm. (based on [8] with permission of the Combustion Institute).

by detection of changes in infrared radiation produced by the temperature jump of the particles, which occurred with flame appearance. Figure 18 presents ignition data measured in air for 25-μm-diameter coal particles and totally devolatilized coal particles at 7.65 atm. This figure is presented to establish a basis for the discussion of all of their coal-ignition data. This comparison of coal and char ignition results under the same conditions suggests that the heterogeneous oxygen-char reaction can be neglected as long as volatiles are being generated by pyrolysis of the coal particles.

Figure 19 is a summary plot of the coal ignition data in air at 7.65 atm for average particle diameters of 12, 25, 48.5, and 96.5 μm. The results are presented in terms of the calculated

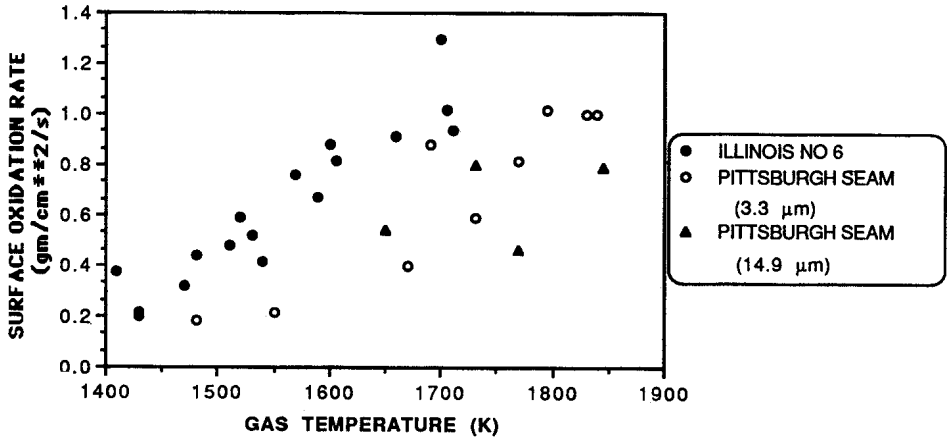


**Figure 17.** Surface oxidation rates behavior with gas temperature. $P_O$ = 1.6 atm, $P_N$ = 6.4 atm. (based on [8] with permission of the Combustion Institute).

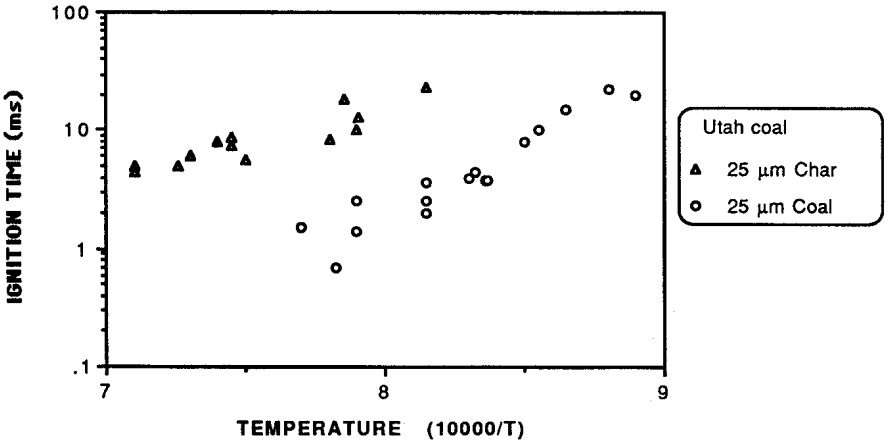


**Figure 18.** Ignition times in air against the reciprocal of the calculated gas temperature behind the reflected shock wave (based on [9] with permission of the Combustion Institute).

gas temperature, and the ignition times have been corrected to account for the fact that the measured times were relative to the time that the incident shock wave reached the end of the tube, while the total particle heating time would start when the particle first entered the hot stagnant gases. An estimate of the magnitude of this time correction suggests that the measured times were too long by about 0.2 ms, and tests in which very high shock strengths were used to induce very rapid ignition indicated a correction of 0.5 ms. A correction of 0.3 ms was adopted, but an uncertainty of about 0.2 ms must be accepted in the ignition times of [9].

An important effect noted in the data shown in Figure 19 is that under similar test conditions, the ignition times were increased by almost a factor of five when the particle size was

increased by a factor two. Such a strong function of particle size on ignition times has not been previously established. Two points in Figure 19 are for a mixed-size sample of equal masses of each of four sizes (96.5, 48.5, 40.5, and 25-$\mu$m) of coal particles. Much as expected, the ignition times for the mixed sample, as measured by first light, corresponded to the ignition times of the smaller (25-$\mu$m diameter) particles. This result emphasizes that under the shock tube test conditions, little interaction occurred between particles.

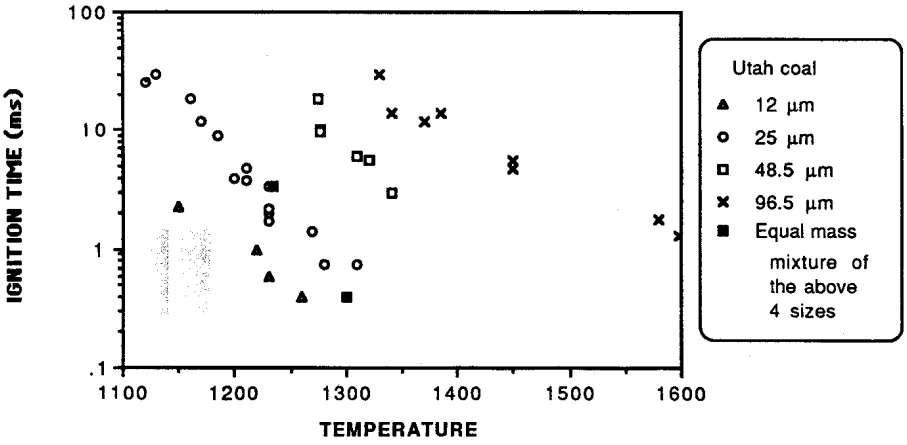


**Figure 19.** Ignition times of coal particles of various sizes in air as a function of the calculated gas temperature behind the reflected shock wave (based on [9] with permission of the Combustion Institute).

In the above three cases [1, 8, 9], a plate of a knife blade was installed inside the shock tubes to contain dust samples. And the reflector was located 18–27 cm behind the knife blade, resulting in the exposure of the dusts to the incident shock wave condition long enough not to have an influence. Therefore, the ignition delay times in hot stagnant gas could not be obtained in those cases.

This shortcoming has been improved in [6]. To disperse the dusts across the cross section of the shock tube, a new air injector was devised, which injected dusts into the shock tube when a shock wave arrived at it. The reinforced air injector is schematized in Figure 20. Furthermore, the reflector was placed 1.5 cm behind the air injector to reduce the effects of forced convective flow induced by the incident shock wave to a minimum. The ignition delay time was defined as the time interval between the interaction of the reflected shock wave with the dust cloud and the appearance of visible light.

Typical cloud interaction with a shock wave is illustrated in Figure 21. As is shown in the figure, after a collision of the dust with the shock wave, the particles moved downstream a little. And the incident shock wave was reflected by a reflector installed on the right-hand side. The size ranges of the dusts investigated are listed in Table 2. Their typical magnified photographs of shapes are represented in [6]. As can be seen, their shapes are very irregular.

In Figure 22, their experimental ignition delay times are plotted on a logarithmic scale versus the inverse reflected shock gas temperature, nondimensionalized by the initial temperature together with its corresponding incident shock wave Mach number. The raction rate of the particle depends on the rate of transport of oxygen by diffusion to the particle. To prevent the whole phenomena from being controlled by the diffusion of oxygen to the parti-

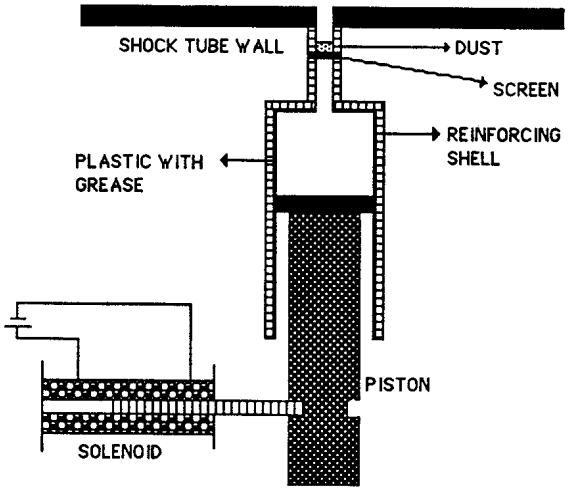


**Figure 20.** Schematic of a reinforced air injector (reprinted from [6] with permission of Gordon and Breach Science Publishers Inc.).

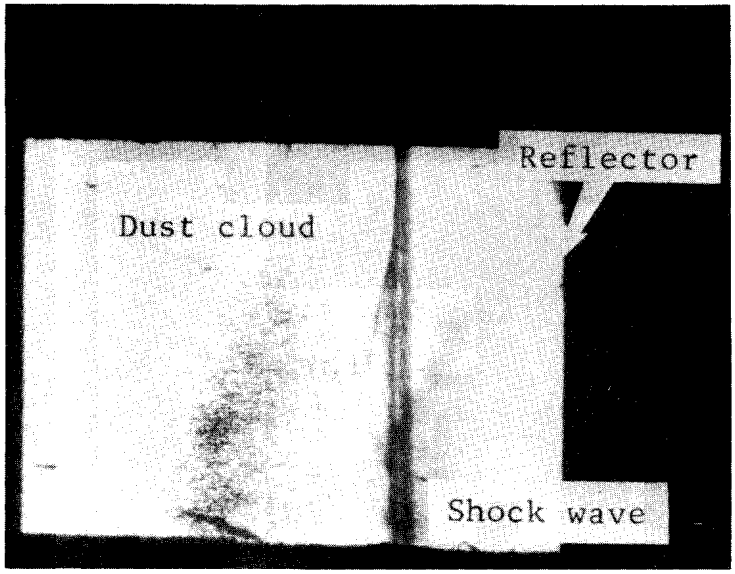


**Figure 21.** Shadowgraph of dust/shock wave interaction for 53 – 74 $\mu$m coal dust, incident shock wave Mach number, M = 3.19 (reprinted from [6] with permission of Gordon and Breach Science Publishers Inc.).

**Table 2**
**Dusts Investigated**

| Substance | Particle-Size Range ($\mu$m) |
|---|---|
| Coal (Pittsburgh Seam) | 53–74 |
| Oats | 53–74 |
| Corn Starch | 53–74 |
| Flour | 53–74 |
| Wheat | 53–74 |
| Lycopodium | Less than 34 |

*Reprinted from [6] with permission of Gordon and Breach Science Publishers Inc.*

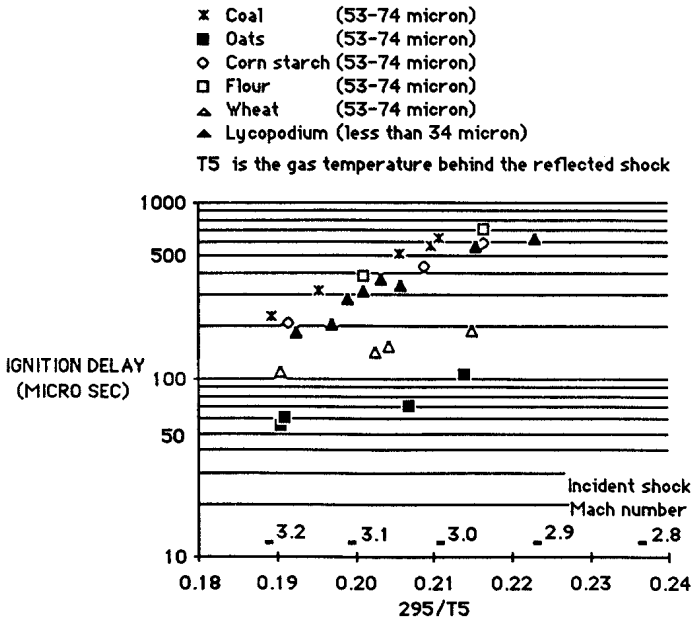


**Figure 22.** Experimental ignition delay under reflected shock conditions (reprinted from [6] with permission of Gordon and Breach Science Publishers Inc.).

cle, all experimental data presented were obtained with pure oxygen at an initial pressure of 1/3 atm in the test section. Therefore, only thermal effects on the particle ignition were sought.

As was expected generally, the ignition delay time in the figure decreases with increasing gas temperature. All ignition delays are above 100 $\mu$sec except for that of oats dust. But it was observed that coal, as well as oats, under reflected shock condition was ignited much

later than under incident shock conditions [4]. This difference is due to the absence of strong convective heating behind the reflected shock wave.

In [15], to assess the detonability of heterogeneous mixtures, their ignition delays were measured behind the reflected shock waves. The experiments were carried out with powders of aluminum (particle sizes between 15 and 20 $\mu$m), TNT (100-$\mu$m particles), naphtalene, and wheat flour. The ignition delays were compared with those for kerosene drops in air and for gaseous mixtures of heptane and methane. Figure 23 presents the measured ignition delays of these different combustible powders. As follows from the figure, the ignition delays of dusts in reflected shock waves are close to those for liquid fuel drops and are much larger than for gases.

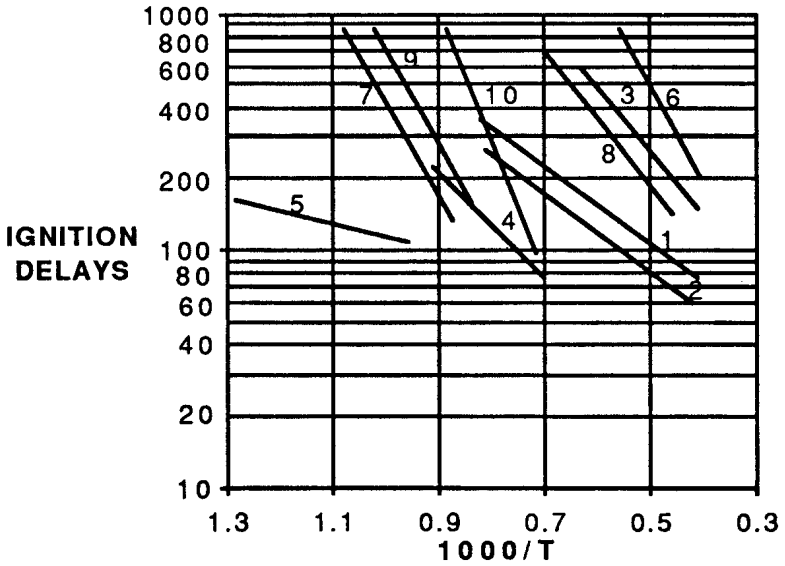


**Figure 23.** Arrhenius plots of ignition delays of dust suspensions (data from [15]).

1. TNT-air
2. Wheat flower
3. Naphthalene
4. Coal dust-$O_2$
5. RDX-$O_2$
6. $C_{17}H_{34}$-air
7. Kerosene-$O_2$
8. Aluminum
9. Heptane-air
10. Methane-air

*Ignition in Fluidized Bed Combustor*

Recently, Prins et al. [41] reported on volatiles and char ignition delays. They investigated four coal types, as listed in Table 3.

The time from the introduction of a coal particle into the fluidized bed until the visible appearance of a volatile flame is called the volatiles ignition delay. Table 4 shows, for coal type 2, that the ignition delay increases with decreasing bed temperature. Also, coal particles twice as large were found to yield somewhat longer ignition delay, and wet coal particles (as received) cause the volatiles ignition delay to be several times larger than that for air-dried coal particles. The effect of moisture content is obvious, since the production of combustible volatiles is retarded by the evaporation of water, which has a considerable heat effect.

The char ignition delay is largely determined by the bed temperature as in Figure 24. Char delay times depend on the type of coal. At a relatively low bed temperature (600°C), the char ignition delay of high-rank coals appears to be larger than that of low-rank coals. This could result from the difference in reactivity with respect to the carbon/oxygen reaction. At a high bed temperature (800°C), low rank coals show the largest ignition delay. The transition of behavior must be related to the process of volatiles evolution. At a low bed temperature, solid ignition of the partially devolatilized coal particle occurs faster than that of the volatiles free char particle. At a high bed temperature, however, the rapid devolatilization and subsequent combustion of volatiles hinders the char ignition.

**Table 3**
**Coal Analyses**

| | 1 | 2 | 2* | 3 | 3† | 4 |
|---|---|---|---|---|---|---|
| Proximate Analysis (%) | | | | | | |
| Moisture | 12.6 | 16.4 | 48.5 | 1.9 | 0 | 1.3 |
| Volatile matter | 48.0 | 33.9 | 20.9 | 35.3 | 0 | 11.3 |
| Ash | 4.1 | 24.0 | 14.8 | 19.2 | 30.5 | 4.6 |
| Fixed carbon | 35.3 | 25.6 | 15.8 | 43.7 | 69.5 | 82.7 |
| Ultimate Analysis (%) | | | | | | |
| Carbon | 65.6 | 39.9 | 24.6 | 64.9 | 80.6 | 87.4 |
| Hydrogen | 3.9 | 3.8 | 2.3 | 3.4 | 5.4 | 3.8 |
| Nitrogen | 0.7 | — | — | 0.9 | 1.6 | 0.9 |
| Sulfur | 0.2 | 1.0 | 0.6 | 0.8 | 0.7 | 0.3 |
| Oxygen | 12.8 | 14.9 | 9.2 | 9.0 | 5.6 | — |
| Chlorine | 0.1 | — | — | 0.1 | 0.2 | 0.1 |

* *Wet brown coal, type 2 as received.*
† *Char of type 3, prepared in a nitrogen fluidized bed at 850°C.*
*Reprinted from [41] with permission of the Combustion Institute.*

**Table 4**
**Volatiles Ignition Delay**

| Bed Temperature (C) | Coal Type | Particle Diameter (mm) | Ignition Delay (S) |
|---|---|---|---|
| 680 | 2 | 4.7 | 9.0 |
| | 2 | 8.6 | 17.6 |
| | 2* | 9.3 | 45.8 |
| 750 | 2 | 4.7 | 2.8 |
| | 2 | 8.6 | 3.3 |
| | 2* | 9.3 | 19.2 |
| 850 | 2 | 4.7 | 1.2 |
| | 2 | 8.6 | 2.6 |
| | 2* | 9.3 | 10.9 |

*Bed material: low-density alumina; oxygen mole fraction: 0.21; fluidization velocity: 0.25 m/s.*
*Reprinted from [41] with permission of the Combustion Institute.*

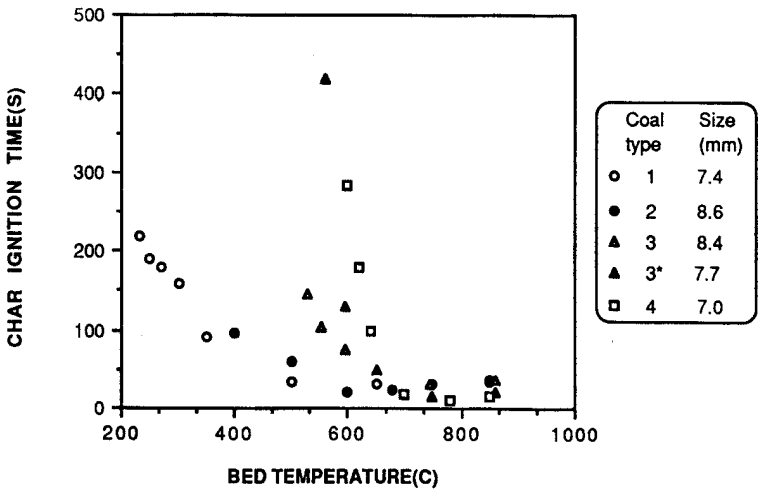


**Figure 24.** Char ignition delay as a function of the bed temperature for five different coal types (reprinted from [41] with permission of the Combustion Institute). Bed material: low-density alumina; Fluidization velocity: 0.25 m/s; Oxygen mole fraction: 0.21.

## THEORIES

### Introductory Remarks

Among the many papers published that have developed ignition theories, [16] presented a review of the classical literature and thermal ignition theory. Reference [28] calculated the variation of ignition position and ignition delay time for different geometries, i.e., a slab, a cylinder, and a sphere, using Frank-Kamenetskii parameters and different wall temperatures. It was concluded that if the scale of the reaction zone is much smaller than the characteristic length of the body size, then infinite body theory can be used to estimate the ignition delay; otherwise the theory is not applicable.

Generally speaking, existing theoretical models for the ignition of a condensed material can be classified into three types, depending on the site of the key exothermic reaction leading to ignition. These are solid-phase, gas-phase, and heterogeneous exothermicity.

### Type of Ignition

For *solid-phase ignition* of a reactive solid, the widely used Zeldovich thermal ignition theory takes into account the heat transfer from the environment and the ensuing heat release but excludes the effects of gas diffusion. This theory has also been applied to the fields of thermal explosion and the ignition of solid propellants. Reference [17] presented the results and correlations of a numerical analysis. An asymptotic analysis for the limit of large activation energy, which has been recently developed for combustion science, was applied to various types of ignition of a condensed material in the solid phase [18–20, 42].

For *heterogeneous ignition*, including the diffusion effects of the oxidizer, the asymptotic analysis for the limit of large activation energy was also applied [21–24]. Meanwhile, [25] used a local similarity method and other related methods to analyze the problem.

In *gas-phase ignition*, a process of endothermic gasification, which is usually assumed to be of an Arrhenius type, as well as the diffusion effects of the oxidizer, must be included. It was found that in this type of ignition there are three different stages: the inert, transition, and transport-controlled stages. Depending on the temperature at which fuel vapor is generated, the ignition process occurs during the transition or transport-controlled stage. Each case has been analyzed in [26, 27]. All of the above asymptotic analyses were done for a semi-infinite body.

It is desirable to identify which type of ignition actually occurs in a given situation. To clarify this, [29] opened the way for direct comparison of the heterogeneous and gas-phase theories on a more or less equal basis with each other by extending the solution of [30] to the heterogeneous case. The results showed, however, that both theories give similar predictions for the ignition delay time. Therefore, the experimental results were incapable of identifying the correct theory of ignition. Also, the problem of the transition of ignition from one mode to another was addressed in [31]. It was theorized that for a partially pyrolysive material like coal, the mode of ignition varies depending on the particle size, volatile content, and ambient oxygen concentration. However, there is still no satisfactory theory that explains what type of ignition mode is more significant in a given situation.

### Definition of Ignition

Definition of ignition is another difficulty in both experimental and theoretical work. Reference [17], in its numerical study, defined the nondimensional ignition time as the nondimensional heating time required for the surface temperature to reach a minimum in an additional time equal to the initial heating time after cessation of heating. In thermal theory, a widely used definition of ignition delay is the time when a precipitous change of the temperature occurs.

### An Elementary Model

The simplest model of ignition is the basis for the elementary theory. Its characteristic features are as follows:

1. The thickness of the heated layer in which the chemical reaction proceeds is considerably less than the radius of particle, so that the particle may be visualized as a semi-infinite body with flat surface.
2. The physical properties are constant throughout the process.
3. The chemical reaction is of the zeroth order.

The equation for the elementary model is then denoted by

$$\frac{\partial T}{\partial t} = \alpha \frac{\partial^2 T}{\partial x^2} + \frac{Q}{\rho c} A \exp\left(-\frac{E}{RT}\right) \tag{1}$$

The initial condition is $t = 0$, $T = T_i$. The boundary conditions are as follows:

$$\text{at } x = \infty \qquad \frac{\partial T}{\partial x} = 0$$

$$\text{at } x = x_s \qquad -\lambda \left(\frac{\partial T}{\partial x}\right)_s = q_o = \text{constant or } T_s = T_o$$

depending on the heating mechanism.

For a case of ignition at a constant surface temperature, the formula for $t_i$, ignition delay time is

$$\ln \frac{t_i}{T_o - T_i} = \frac{E}{RT_o} + \ln \left[ 0.2 \frac{\rho c}{QA} \left( \frac{E}{R} \frac{T_o - T_i}{T_o^2} + 8 \right) \right] \tag{2}$$

For the ignition by a constant heat flux, $t_i$ can be represented by

$$t_i = 0.46 c\rho\lambda (T_b - T_i)^2 \left[ 1 + \frac{12RT_b^2}{E(T_b - T_i)} \right] q_o^{-2} \tag{3}$$

as in [16] where $T_b$ is the temperature of inflection of the $T_s(t)$ curve.

**Solid-Phase Ignition under Convective Heating**

Reference [32] dealt with the analytical description of the process of solid-phase ignition of a solid under convective heating by a hot gas. The effects of interphase mass transfer were neglected. When a semi-infinite body is heated at its surface by a flux proportional to the difference in its surface temperature and that of the source, the equations describing the temperature distribution can be written in nondimensional form as the heat conduction equation

$$\frac{\partial \theta}{\partial \tau} - \frac{\partial^2 \theta}{\partial \xi^2} = 0 \qquad \xi > 0,\ \tau > 0 \tag{4}$$

to be solved with the initial condition

$$\theta(\xi, 0) = \theta_i$$

which is also the temperature of the solid far from the surface at all times. The surface condition is

$$\xi = 0,\ \tau > 0: \qquad -\frac{\partial \theta}{\partial \xi} = 1 - \theta + \mathrm{B} \exp\left(-\theta_a/\theta\right) \tag{5}$$

where an exothermic heterogeneous reaction with Arrhenius kinetics takes place at the surface of the solid. The temperature has been made nondimensional with the temperature of the heat source; $\theta_a$ is the nondimensional activation temperature. The characteristic length and time used in the nondimensional length $\xi$, time $\tau$, and frequency factor B have been obtained from the thermal diffusivity, thermal conductivity, and convective heat transfer coefficient. By integrating Equation 4 with initial and boundary conditions, the following integral equation can be obtained between the surface temperature $\theta_s$ and heat transfer flux at the surface:

$$\theta_s - \theta_i = \frac{1}{\sqrt{\pi}} \int_0^{\tau} \frac{1 - \theta_s + \mathrm{B} \exp\left(-\theta_a/\theta_s\right)}{\sqrt{\tau - \eta}}\, d\eta \tag{6}$$

For large values of $\theta_a$ and fast reactions corresponding to large values of $\mathrm{Bexp}(-\theta_a)$, a thermal runaway occurred at a well defined ignition time $\tau_i$, given by the relation

$$B = e^{-0.431}\left(\frac{\theta_{si}^2}{\theta_a \theta_{si}'}\right)^{1/2} e^{\theta_a/\theta_{si}} \tag{7}$$

where $\theta_{si} = \theta_s(\tau_i)$

$$\theta_{si}' = \frac{d\theta_s}{dt}(\tau_i)$$

For large values of $\theta_a$ and slow reactions corresponding to values of B such that $\delta = \theta_a B \exp(-\theta_a)$ is of order unity, the ignition time $\tau_i$ is given by the relation

$$\frac{\theta_a(1-\theta_i)}{\sqrt{\pi\tau_i}} = \ln\{e\theta_a B e^{-\theta_a}\} \tag{8}$$

For subcritical values of $\delta$, that is, for values of B smaller than a critical $B_c$

$$B_c e^{-\theta_a} = \frac{1}{e\theta_a} \tag{9}$$

no ignition time, leading to high temperature, exists.

**Radiant Ignition of Solid**

In [19], an asymptotic analysis of the limit of large activation energy was presented for radiant ignition of a solid that experiences a one-step Arrhenius reaction in the condensed phase. The mathematical problem that must be solved can be written as

$$\frac{\partial\theta}{\partial\tau} = \frac{\partial^2\theta}{\partial\xi^2} + I\zeta\exp(-\zeta\xi) + A(1-\epsilon)^b \exp(-\theta_a/\theta) \tag{10}$$

and

$$\frac{\partial\epsilon}{\partial\tau} = \frac{A}{B}(1-\epsilon)^b \exp(-\theta_a/\theta) \tag{11}$$

with the initial conditions

$$\epsilon(\xi,0) = 0 \qquad \theta(\xi,0) = 1$$

and the boundary conditions

$$\epsilon(\infty,\tau) = 0 \qquad \theta(\infty,\tau) = 1 \qquad \frac{\partial\theta}{\partial\xi}(0,\tau) = 0$$

The initial temperature $T_o$ of the solid is taken to be uniform. The ratio of $\lambda T_o$ to the nonreflected portion q of the incident radiant energy flux at ignition will be employed as the char-

acteristic length in forming the nondimensional spatial variable $\xi$. The quantity $(\lambda T_o/q)^2/\alpha$ is the characteristic heat conduction time that will be used to form the nondimensional time variable $\tau$. Dependent variables are $\theta(\xi,\tau) = T/T_o$ and $\epsilon(\xi,\tau)$, the ratio of the product concentration to the final product concentration. Nondimensional parameters that appeared are a Damköhler number A, defined as the ratio of the characteristic heat conduction time to a characteristic chemical time, the latter being based solely on the pre-exponential rate factor; the nondimensional activation energy $\theta_a = T_a/T_o$, where $T_a$ is the activation temperature, the order b of the chemical reaction, and the heat release parameter $B = (T_f - T_o)/T_o$, where $T_f$ is the adiabatic flame temperature of the ignition reaction. The additional nondimensional absorption coefficient is defined as $\zeta = \mu\lambda T_o/q$ where $\mu$ is the absorption coefficient. The function $I(\tau)$ is defined as the ratio of the instantaneous incident radiant flux to the incident radiant flux at ignition. For clarity of presentation, $I(\tau) = 1$ is assumed here.

When the order of $\zeta$ is the same as that of $\theta_a$, the thermal runaway or ignition was found to occur at $\tau_c$:

$$A \exp\left(-\frac{\theta_a}{\theta_c}\right) = \left(\frac{\theta_a}{\theta_c^2}\right)^{1/2} (\pi\tau_c)^{-1/4}\, G^{-1} \exp(d_o) \tag{12}$$

where G is a function of $\zeta_1$, defined by

$$G = \int_0^\infty \exp[-x - \zeta_1^{-1} \exp(-\zeta_1 x)]\, dx \tag{13}$$

$\zeta_1$ is of order unity and defined as $\zeta_1 = \zeta\delta^2$, where $\delta = \sqrt{\theta_c^2/\theta_a}$; $d_o$ in Equation 12 is expressed as $d_o = d_o' + \ln G$. $d_o'$ is the first term of an expansion

$$d = d_o' + \delta d_1' + \ldots \tag{14}$$

of the quantity

$$d = \ln\left[(\pi\tau_c)^{1/4} \left(\frac{\theta_c^2}{\theta_a}\right)^{1/2} A \exp\left(\frac{-\theta_a}{\theta_c}\right)\right] \tag{15}$$

$\theta_c$ is expressed as

$$\theta_c = 1 + 2\sqrt{\tau_c/\pi} - \zeta^{-1}(1 - g_c) \tag{16}$$

where

$$g_c = \exp(\zeta^2\tau_c)\, \mathrm{erfc}\left(\zeta\sqrt{\tau_c}\right) \tag{17}$$

When $\zeta$ is on the order of unity, the thermal runaway or ignition was found to occur at $\tau_c$:

$$A \exp\left(-\frac{\theta_a}{\theta_c}\right) = \zeta g_c \exp(c_o) \tag{18}$$

where $c_0$, which is of order unity, is the first term of the expansion

$$c = c_0 + \delta^2 c_1 + \ldots \tag{19}$$

of the quantity

$$c = \ln [\zeta^{-1} g_c^{-1} A \exp(-\theta_a/\theta_c)] \tag{20}$$

**Ignition of Solid in Stagnation Point Flow**

Reference [20] developed a theory to describe ignition of a solid body that is quickly immersed in the flow of a hot gas. The homogeneous solid, semi-infinite in extent, experiences a one-step reaction of the Arrhenius type without reactant depletion. The problem, as shown schematically in Figure 25, has the constant-property condensed phase occupying the half-space $x<0$ and the stagnation-point flow of the inert, ideal gas occupying the half space $x>0$. Since the gas efflux is neglected during the ignition transient, the solid-gas interface remains fixed at $x = 0$. As in [20], the well-known set of ordinary differential equations for quasi-steady flow model, obtained after performing the Howarth-Dorodnitzyn transformation, is

$$f''' + ff'' + \frac{1}{k+1}(\theta/\theta_e - f'^2) = 0 \tag{21}$$

$$\theta'' + f\theta' = 0 \tag{22}$$

with boundary conditions $f = f' = 0$, $\theta = \theta_0$ at $x = 0$; and $f' = 1$, $\theta = \theta_e$ at $x = \infty$, in which f and $\theta$ are nondimensional stream function and nondimensional gas-phase temperature equal to $T/T_i$, and primes denote the differentiation with respect to the similarity variable

$$\eta = \{(k+1)t_f \rho_e c_e/\lambda_e\}^{1/2} \int_0^x \rho/\rho_e dy$$

In the above equations, $t_f$ is the characteristic flow time and k is a constant equal to 0 for two-dimensional flows and equal to 1 for axisymmetric flows. The Prandtl number was taken as unity, the specific heat c at constant pressure is treated as constant, and the equality $\rho\mu = \rho_e\mu_e$ was assumed.

The energy equation for the solid and the associated boundary and initial conditions can be written in nondimensional form as

$$\frac{\partial \psi}{\partial \tau} = \frac{\partial^2 \psi}{\partial \xi^2} + A \exp\left(-\frac{\psi_a}{\psi}\right) \tag{23}$$

$$\frac{\partial \psi}{\partial \xi}(0,\tau) = \theta_e - \psi(0,\tau), \quad \psi(\xi,0) = \psi(-\infty,\tau) = 1$$

where $\psi_a$ is the nondimensional activation energy equal to $E/RT_i$.

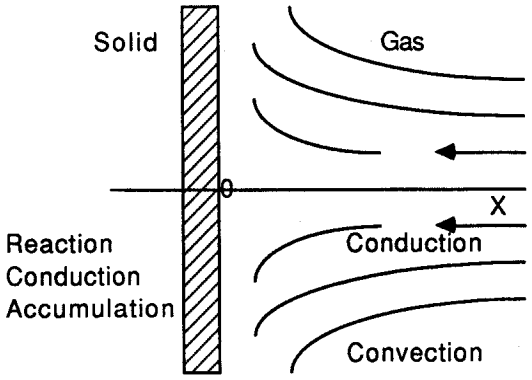


**Figure 25.** Schematic diagram of the configuration for the problem (adapted from [20] with permission of Gordon and Breach Science Publishers Inc.).

For the previous formulations, an implicit formula for the ignition time, $\tau_c$, was found to be

$$\frac{A}{(\theta_e-1)^2}=e^{-0.431}\sqrt{\psi_a}\,g_c\left[\frac{1}{\sqrt{\pi\tau_c^*}}-\frac{g_c}{\theta_e-1}\right]^{1/2}\frac{1}{1+(\theta_e-1)\,(1-g_c)}$$
$$X\exp\left\{\frac{\psi_a}{1+(\theta_e-1)\,(1-g_c)}\right\} \tag{24}$$

where

$$g_c=\exp\left[\tau_c^*(\theta_e-1)^{-2}\right]\operatorname{erfc}\left[\sqrt{\tau_c^*}\,(\theta_e-1)^{-1}\right] \tag{25}$$

$$\tau_c^*=\tau_c(\theta_e-1)^2$$

## Shock Wave Ignition of Dusts

### *Incident Shock Wave Ignition*

*Numerical Analysis.* A physically plausible model for the ignition of dust behind a moving shock wave has been described in [4]. The ignition process was simulated starting from the instant the shock wave passes over a dust particle until ignition occurs.

For a particle that is initially in a convective flow behind the shock, the equation of motion is

$$\frac{4}{3}\pi R_p^3\rho\,\frac{dV_p}{dt}=\frac{1}{2}C_d\rho_2\pi R_p^2\,(V_2-V_p)^2 \tag{26}$$

where $\rho$ and $\rho_2$ = particle and gas densities
$V_p$ and $V_2$ = particle and gas flow velocities
$R_p$ = particle radius
$C_d$ = drag coefficient

When the relative velocity $(V_2 - V_p)$ is supersonic, a bow shock forms in front of each particle, as shown in Figure 26. In Equation 26, the empirical correlation given in [33] was used for the drag coefficient $C_d$. In Figure 27, the numerically calculated relative Mach number is plotted versus time for two sizes of coal particles, starting from the interaction with the incident shock wave. For the same incident shock wave strength, the acceleration of the smaller particles is greater than that of the larger.

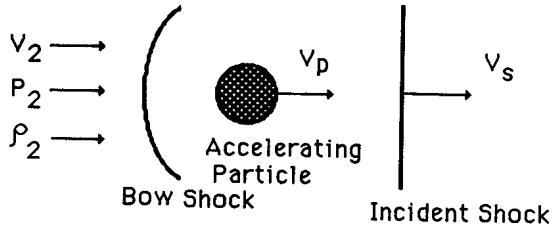


**Figure 26.** Schematic of interaction of a shock with a particle.

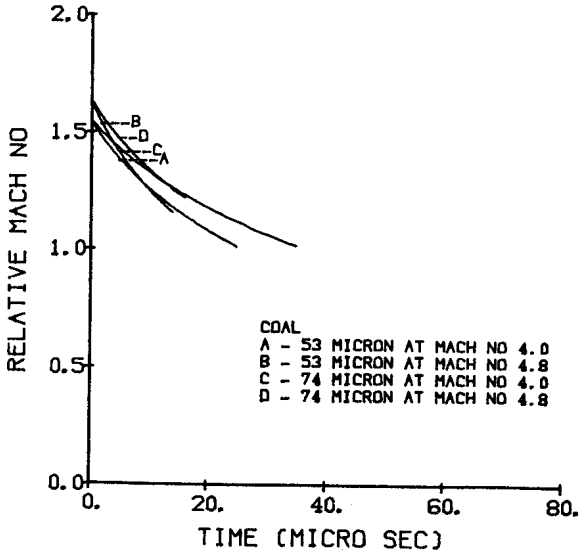


**Figure 27.** Variation of relative Mach number with time for 53- and 74-micron coal particles (reprinted from [4] with permission of the American Institute of Aeronautics and Astronautics).

The unsteady heat conduction equation inside a particle with a reactive heat source can be expressed as

$$\frac{\partial T}{\partial t} = \frac{\alpha}{r^2}\frac{\partial}{\partial r}\left(r^2\frac{\partial T}{\partial r}\right) + \frac{u'''(r,t)}{\rho c} \tag{27}$$

It has been assumed that the particles are spherical and monodisperse and that the particle temperature distribution is spherically symmetric. The volumetric rate of heat generation, $u'''$, is

$$u''' = Q\rho S_i P_{O_2}^n A \exp\left(-\frac{E}{RT}\right) \tag{28}$$

where Q and $S_i$ are the heat of combustion and the internal surface area per unit mass, respectively. $P_{O_2}^n$ is the partial pressure of oxygen of order n. The boundary conditions at the surface and the center of particle become

$$\lambda\frac{\partial T}{\partial r}(R_p,t) = h(t)[T_f(t) - T(R_p,t)] \tag{29}$$

$$\frac{\partial T}{\partial r}(0,t) = 0 \tag{30}$$

The initial condition is $T = T_i = 295$ K. In Equation 29, an empirical correlation of experimental data developed by [34] was used to determine the convective heat transfer coefficient h(t). Equations 26 through 30 have been solved numerically for coal with $n = 1$ according to [14] and oats with $n = 1/2$ according to [35]. All of the data for the thermal and chemical kinetic properties used in the computation of ignition delay times of coal and oats are summarized in Table 5.

Typical temperature profiles for the interior of a 53-micron coal particle at $M = 4.8$ are shown in Figure 28, where RR is the outer radius of the particle and R is the radial coordinate. Only part of the particle radius, corresponding to three tenths of the radius from particle surface, is shown on the abscissa. The rate of surface-temperature increase slows down initially, but then increases due to the effects of reaction. The occurrence of ignition is represented by temperature runaway. The computed ignition delay times for coal and oats are shown in Figures 29 and 30 respectively, and are denoted by number 2.

*Characteristic Time Approach.* The ignition delay times can be estimated by incorporating the key parameters relevant to the physically intrinsic concepts into a definition of ignition. In terms of characteristic times, two simplified methods for the calculation of ignition delay times are introduced here.

Through the integration of the trajectory Equation 26, the *characteristic acceleration time*, $\tau_a$, can be defined as

$$\tau_a = \frac{R_p/V_2}{\frac{3}{8}C_d\frac{\rho_2}{\rho}} \tag{31}$$

**Table 5**
**Thermal and Chemical Kinetic Properties of Coal and Oats Dust**

| Variable | Coal | Oats |
|---|---|---|
| Density ($g/cm^3$) | 1.2 | 0.75 [1] |
| Thermal conductivity (cal/cm/s/c) | 0.00212 | 0.0007 [2] |
| Specific heat (cal/g/c) | 0.236 | 0.24 [2] |
| Heat of combustion (cal/g) | 8,559 | 3,040 [3] |
| Internal surface area ($cm^2/g$) | $4.26 \times 10^6$ | $9 \times 10^7$ [4] |
| Activation energy (kcal/gmole) | 35.7 | 37.2 [4] |
| Pre-exponential factor, A ($g/cm^2/s/atm^n$) | 8,710 | 31,000 [5] |

[1] *Estimated based on bulk density of oats.*
[2] *Refer to [35].*
[3] *Refer to [36], average value taken.*
[4] *Based on best fit of computed and measured ignition delays.*
[5] *Based on smoldering combustion measurements in [35].*
*Reprinted from [4] with permission of the American Institute of Aeronautics and Astronautics.*

$\tau_a$ is the order of time required for the particles to accelerate to the gas velocity. As can be seen from the slopes of the curves of particle velocity versus time in Figure 27, for particles of the same size the acceleration time is smaller at higher Mach numbers, and at the same Mach number, it is smaller as well for smaller particles. The acceleration time is closely related to the rate of change of convective heat transfer and to the gas recovery temperature. Figure 31 shows the variations of convective heat transfer coefficient and gas recovery temperature with time for 53- and 74-micron coal particles at M = 4.8. The 53-micron particle having a smaller acceleration time experiences a more rapid change of these parameters.

The *characteristic thermal time*, $\tau_{th}$, can be defined as the time required for the particle surface temperature $T_s$ to reach a given value during convective heating without taking the reactive heat source term into account. Figure 28 shows that the temperature at the center of the particle stayed at the initial temperature $T_i$. An analytic solution of Equation 27 without the heat source term can be found with the boundary condition $T(0,t) = T_i$ instead of Equation 30. For constant average values of convective heat transfer coefficient, h, and gas recovery temperature, $T_f$, it follows that

$$T = T_f + \frac{1}{r} \sum_{n=1}^{\infty} \beta_n \sin(\omega_n r) \exp(-\alpha \omega_n^2 t) \tag{32}$$

where $\omega_n$ are eigenvalues determined by

$$\tan(\omega_n R_p) = -\frac{\omega_n}{W} \text{ and } W = \frac{h}{\lambda} - \frac{1}{R_p}$$

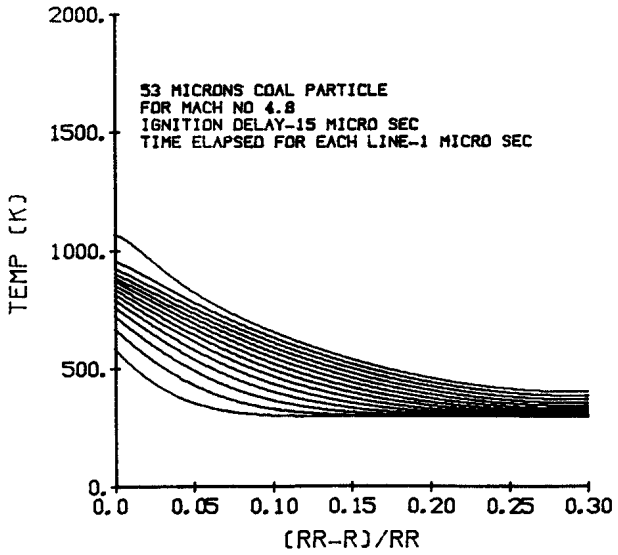


**Figure 28.** Temperature variation with time along radial direction for 53-micron coal particle along the radial direction under incident shock condition created by incident shock wave Mach number, M = 4.8 (reprinted from [6] with permission of Gordon and Breach Science Publishers Inc.).

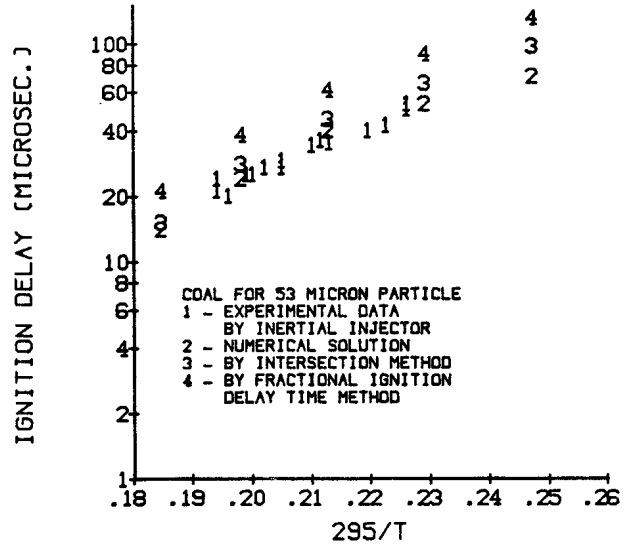


**Figure 29.** Comparison of computed and measured ignition delays for coal dust (reprinted from [4] with permission of the American Institute of Aeronautics and Astronautics).

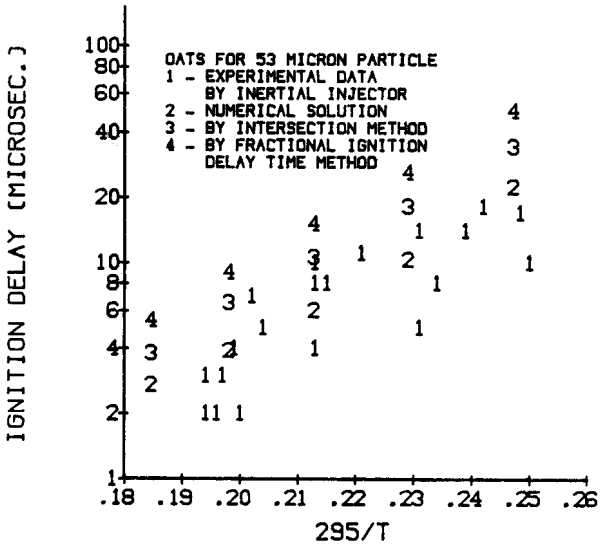


**Figure 30.** Comparison of computed and measured ignition delays for oats dust (reprinted from [4] with permission of the American Institute of Aeronautics and Astronautics).

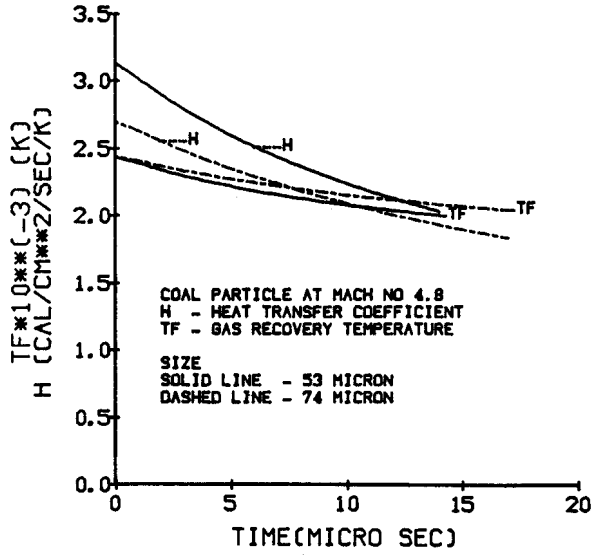


**Figure 31.** Variation of convective heat transfer coefficient and gas recovery temperature with time for 53- and 74-micron coal particles at M = 4.8.

The coefficients $\beta_n$ are given by

$$\beta_n = \frac{4\left(T_i - \dfrac{Z}{1+WR_p}\right)\left[\dfrac{\sin(\omega_n R_p)}{\omega_n} - R_p\cos(\omega_n R_p)\right]}{2\omega_n R_p - \sin(2\omega_n R_p)}$$

$$\text{and } Z = \frac{hR_p}{\lambda} T_f$$

Using Equation 32, the particle surface temperature variation with time, $T_s = T(R_p,t)$, was plotted in Figures 32 and 33 for 53-micron coal and oats particles. Each value of t can be considered as the thermal time, $\tau_{th}$, corresponding to the particle surface temperature, $T_s$, at time t.

Using Equation 7, a characteristic chemical time, $\tau_{ch}$, can be defined as

$$\tau_{ch} = \left[\exp\left(-\frac{E}{RT}\right) S_i P_{O_2}^n A\right]^{-1} \tag{33}$$

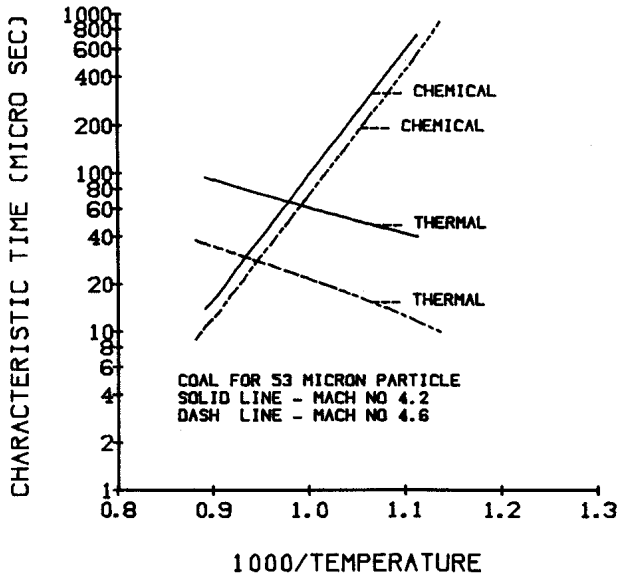


**Figure 32.** Variation of characteristic thermal and chemical time with the inverse surface temperature for 53-micron coal particles (reprinted from [4] with permission of the American Institute of Aeronautics and Astronautics).

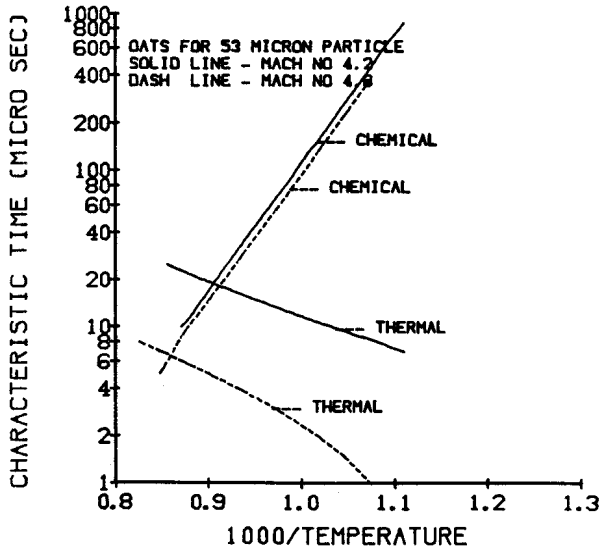


**Figure 33.** Variation of characteristic thermal and chemical time with the inverse surface temperature for 53-micron oats particles (reprinted from [4] with permission of the American Institute of Aeronautics and Astronautics).

For low values of the surface temperature, $T_s$, the chemical time, $\tau_{ch}$, will be much larger than the thermal time, $\tau_{th}$, as is evidenced from Figures 32 and 33, which show the variation of $\ln(\tau_{ch})$ with inverse temperature. As expected, these curves display the typical Arrhenius behavior. With increasing surface temperature, the thermal time increases rather slowly, while there is a precipitous decrease in $\tau_{ch}$ which is characteristic of high activation energy systems. This behavior suggests that ignition will occur soon after $\tau_{ch}$ becomes less than $\tau_{th}$.

The *intersection method* is a simplified approach to the determination of ignition delay time such that the time at the point of intersection where $\tau_{th} = \tau_{ch}$ is chosen. The results of this approach, which is equivalent to the intersection of an ignition temperature, are shown in Figures 29 and 30 as the curves denoted by number 3, and agreement with experimental results is quite good.

Another simplified approach to the calculation of the ignition delay time, which can be termed the *fractional ignition delay time method*, is based on the procedure employed by [37, 38]. If the temperature were constant, $\tau_{ch}$ would be of the order of the ignition delay time, and during interval dt, $(dt/\tau_{ch})$ represents the fraction of the elapsed ignition delay time. Thus

$$\int_0^{\tau_{ig}} \frac{dt}{\tau_{ch}} = 1 \tag{34}$$

if $\tau_{ch} = \tau_{ig}$. This trivial result can be extended to the case in which $\tau_{ch}(T)$ is a function of the temperature, with $T = T_s(t)$ determined by Equation 32 evaluated at the surface of particle, $r = R_p$. Thus the ignition delay time can be determined from the integral relation

$$\int_0^{\tau_{ig}} \frac{dt}{\tau_{ch}(T)} = 1 \qquad T = T_s(t) \tag{35}$$

In this method, the characteristic thermal time, $\tau_{th}$, is actually coupled to the characteristic chemical time, $\tau_{ch}(T)$, implicitly through its argument T. In Figures 34 and 35, the inverse of $\tau_{ch}$ is shown for 53-micron coal and oats dust, respectively, at various Mach numbers. Because of the rapid increase of $(1/\tau_{ch})$ after a given elapsed time, Equation 35 will lead to a fairly sharp definition of $\tau_{ig}$. The corresponding calculated ignition delay times are shown in Figures 29 and 30, and are denoted by number 4.

*Asymptotic Analyses.* The ignition of a solid spherical particle exposed to the hot gas at its surface with constant average values of convective heat transfer coefficient, h, and gas recovery temperature, $T_f$, was investigated using the large activation energy asymptotics in [39].

Using the following nondimensionalized parameters,

$$\theta = \frac{rT}{R_p T_i} \qquad \tau = \frac{\alpha t}{R_p^2} \qquad \xi = \frac{r}{R_p}$$

$$E' = \frac{E}{RT_i} \qquad B_i = \frac{hR_p}{\lambda} \qquad A' = \frac{Q\rho S_i P_{O_2}^n A R_p^2}{\lambda T_i} \tag{36}$$

Equation 27 is transformed into

$$\frac{\partial\theta}{\partial\tau} = \frac{\partial^2\theta}{\partial\xi^2} + A'\xi\exp\left(-\frac{E'\xi}{\theta}\right) \tag{37}$$

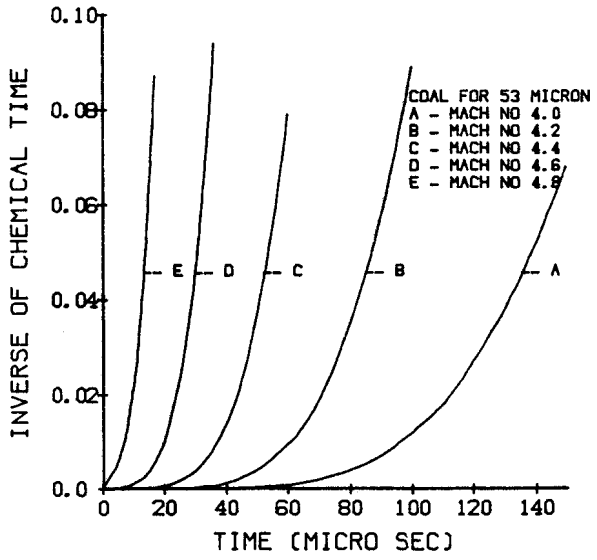


**Figure 34.** Variation of inverse chemical time with time for 53-micron coal particles (reprinted from [4] with permission of the American Institute of Aeronautics and Astronautics).

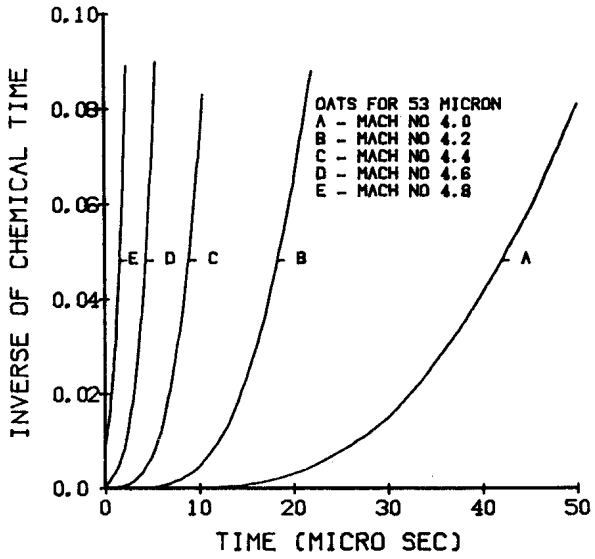


**Figure 35.** Variation of inverse chemical time with time for 53-micron oats particles (reprinted from [4] with permission of the American Institute of Aeronautics and Astronautics).

Then by carrying out an asymptotic analysis for the limit of large activation energy, the thermal runaway was found to occur at $\sigma = b_0 = -0.431$. Using $\sigma = -0.431$, the ignition time $\tau_c$ can be calculated from the following:

$$\theta_c = \theta_I(1,\tau_c) = \frac{Z}{1+X} + \sum_{n=1}^{\infty} \beta_n \sin(\lambda_n)\exp(-\lambda_n^2\tau_c) \tag{38}$$

where $X = B_i - 1, Z = \dfrac{B_i T_f}{T_i}$

$$\tan\lambda_n = -\frac{\lambda_n}{X}$$

$$\beta_n = \frac{4\left[1 - \dfrac{Z}{1+X}\right]\left[\dfrac{\sin\lambda_n}{\lambda_n} - \cos\lambda_n\right]}{2\lambda_n - \sin(2\lambda_n)}$$

$$b = \ln\left[A' \; K_2^{-1/2} \; K_1^{-1} \; \delta \exp(-E'/\theta_c)\right] = b_0 + b_1\delta + b_2\delta^2 + \ldots \tag{39}$$

where $\delta = \theta_c/\sqrt{E'}$

$$K_1 = \sum_{n=1}^{\infty} \beta_n \lambda_n \cos\lambda_n \exp(-\lambda_n^2\tau_c)$$

$$K_2 = -\sum_{n=1}^{\infty} \beta_n \lambda_n^2 \sin\lambda_n \exp(-\lambda_n^2 \tau_c)$$

In Equation 38, $\theta_I(\xi,\tau)$ is the inert temperature defined by

$$\theta_I = \frac{Z\xi}{1+X} + \sum_{n=1}^{\infty} \beta_n \sin(\lambda_n \xi)\exp(-\lambda_n^2 \tau) \tag{40}$$

The results for coal dust are displayed in Figure 36 as the curve labeled (*), together with other computed and measured ignition delays. The above asymptotic analysis was in good agreement with the experimental measurements and the numerical solution. However, the main weakness is the need to choose appropriate values for the average recovery temperature and convective heat transfer coefficient.

In the following, another asymptotic analysis in the limit of large activation energies is described for a semi-infinite body. By employing this geometric simplification, the effects of varying gas recovery temperature and convective heat transfer coefficient could be included in the analysis.

When the surface of a semi-infinite body is heated by convection from hot gases at temperature $T_f$, the dimensional heat conduction equation describing the temperature distribution is expressed by

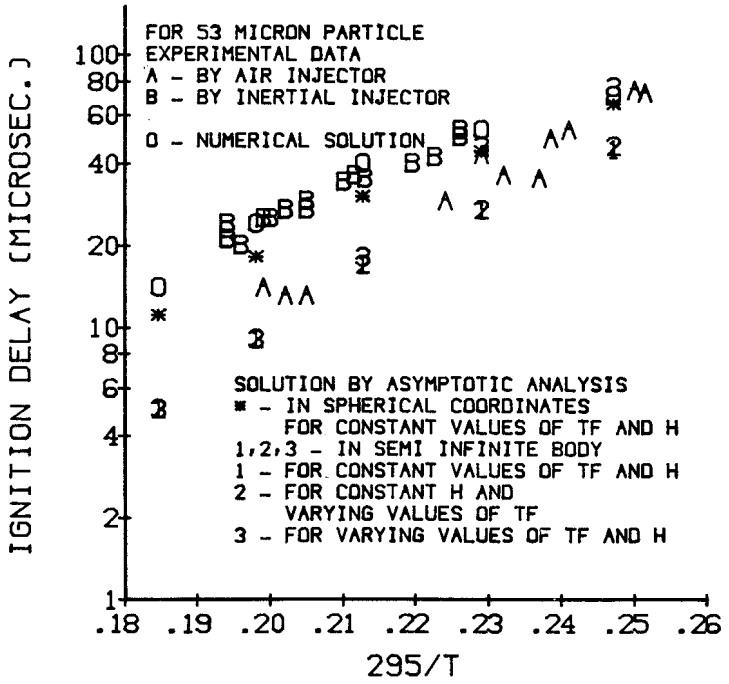


**Figure 36.** Comparison of measured and asymptotically computed ignition delays for coal dust.

$$\frac{\partial T}{\partial t} = \alpha \frac{\partial^2 T}{\partial x^2} \qquad x>0,\ t>0 \tag{41}$$

Under the assumption that an Arrhenius-type exothermic reaction occurs only at the body surface, the boundary condition with a time-dependent gas recovery temperature, $T_f(t)$, and a constant convective heat transfer coefficient, h, can be expressed as

$$-\lambda \frac{\partial T}{\partial x}(0,t) = h[T_f(t) - T(0,t)] + u''$$

where $u''$ is the rate of heat generation per unit area by the exothermic reaction given by

$$u'' = L_{vs} Q \rho S_i P_{O_2}^n A \exp\left(-\frac{E}{RT}\right) \tag{42}$$

The initial condition is $T(x,0) = T_i$.
With the introduction of the following dimensionless parameters

$$\phi = \frac{T}{T_i} \qquad B_o = \frac{h}{\lambda} \qquad E' = \frac{E}{RT_i}$$

$$\phi_f = \frac{T_f}{T_i} \qquad A' = \frac{L_{vs} Q \rho S_i P_{O_2}^n A}{\lambda T_i} \tag{43}$$

Equations 41 and 42, boundary and initial conditions, have been transformed. Then by carrying out an asymptotic analysis for the limit of large activation energy, the ignition delay time $\tau_c$ can be calculated using Equation 44, its derivative at $t_c$, and Equation 45:

$$\phi_c = \phi_I(0,t_c)$$

$$= 1 + \frac{2B_o}{\sqrt{\pi}} \int_0^\infty \exp(-B_o\eta) \int^\infty \frac{\eta}{2\sqrt{\alpha t_c}} \phi_f\left(t_c - \frac{\eta^2}{4\alpha\mu^2}\right) \exp(-\mu^2) d\mu d\eta \tag{44}$$

$$\ln\left[A' \sqrt{\alpha} \exp\left(-\frac{E'}{\phi_c}\right) \sqrt{\frac{E'}{\phi_c^2 \frac{d\phi_I}{dt}(0,t_c)}}\right] = -0.431 \tag{45}$$

In Equation 44, $\phi_I$ is the inert temperature distribution, which is given by

$$\phi_I(0,t) = 1 + \frac{2B_o}{\sqrt{\pi}} \int_0^\infty \exp(-B_o\eta) \int_{\frac{\eta}{2\sqrt{\alpha t}}}^\infty \phi_f\left(t - \frac{\eta^2}{4\alpha\mu^2}\right) \exp(-\mu^2) d\mu d\eta \tag{46}$$

Even if the convective heat transfer coefficient, h, varies with time, the foregoing analysis, which leads to Equation 45, is still valid only if one condition is satisfied, which is expressed in detail in [40]. The effect of varying the heat transfer coefficient, however, is embodied in the calculation of $\phi_c$ and $d\phi_I/dt(0,t_c)$ in Equation 45.

The final results for ignition delay times are plotted in Figure 36, as well, for comparison with the others. The asymptotic analysis of the ignition of a semi-infinite body with a constant average value of gas recovery temperature, $T_f$, yielded shorter ignition delays, but results were still in reasonable agreement with others. When the variation of gas recovery temperature was also taken into account, the results were not significantly different. However, when variations of $T_f$ and h were both taken into account, the predicted ignition delay deviated significantly from the previous results as the incident shock wave strength decreased.

*Reflected Shock Wave Ignition*

The various methods mentioned above in Incident Shock Wave Ignition are still valid in the case of reflected shock wave ignition. In fact, its application is simpler because there is no forced flow around the particle. In this section, thus, as one example, an unsteady thermal history inside a particle in the reflected shock wave conditions is discussed and compared with that in the incident shock wave conditions.

Equation 1, initial and boundary conditions with thermal and chemical properties listed in Table 5 were solved numerically, assuming that only a natural convective heat transfer to the coal particle exists in the reflected shock conditions. The unsteady temperature variation inside a 53-$\mu$m coal particle in the reflected shock conditions is illustrated in Figure 37. In Figure 28, the temperature variation inside a 53-$\mu$m coal particle in the incident shock conditions was shown. RR is the outer radius of the particle and R is the radial coordinate. For the incident shock case, a large surface temperature gradient exists on the surface of particle. And the rate of surface temperature increase initially slows down and then increases due to the effects of surface reaction, with the center of particle remaining at the initial tempera-

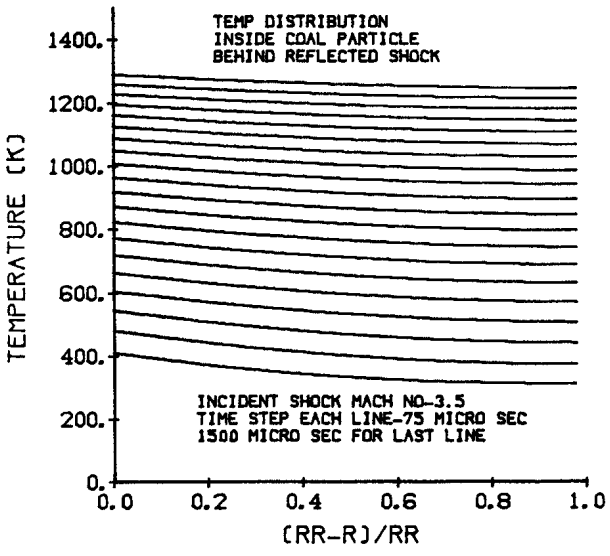


**Figure 37.** Temperature variation with time along radial direction for 53-micron coal particle along the radial direction under reflected shock condition created by incident shock wave Mach number, M = 3.5 (reprinted from [6] with permission of Gordon and Breach Science Publishers Inc.).

ture. Thus, under the incident shock condition, ignition delays of dust were so short that the reaction on the surface of the particle, as well as in pores within the particles, can be considered to be dominant over the gaseous reaction resulting from a devolatilization process. But in a reflected shock case, e.g., hot stagnant gas, the particle temperature is almost uniform at each time along the particle radius and the rate of temperature increase is much slower. Thus, there is enough time for the center as well as the surface of the particle to be heated up uniformly. In this situation, the whole particle is likely to warm up uniformly and be pyrolyzed, so that the volatile gases are ejected in the particle. Then they diffuse from the surface of particle, mix with oxidizer, and finally result in ignition.

## NOTATION

| | | | |
|---|---|---|---|
| A | pre-exponential factor | R | universal gas constant |
| c | specific heat of particle | $R_p$ | radius of particle |
| $C_d$ | drag coefficient | $S_i$ | internal surface area |
| E | activation energy | t | time |
| h | convective heat transfer coefficient | $t_i$ | ignition delay time |
| $L_{vs}$ | volume-to-surface-area ratio | T | temperature |
| M | Mach number | $T_f$ | gas recovery temperature |
| $P^n_{O_2}$ | partial pressure of oxygen of order n | $u'''$ | heat release by the surface reaction |
| $q_o$ | constant heat flux | V | velocity |
| Q | heat of reaction | x | axial coordinate |
| r | radial coordinate | | |

### Greek Symbols

| | | | |
|---|---|---|---|
| $\alpha$ | thermal diffusivity of particle | $\tau_a$ | characteristic acceleration time |
| $\xi$ | nondimensional spatial coordinate | $\tau_{ch}$ | characteristic chemical time |
| $\lambda$ | thermal conductivity of particle | $\tau_{th}$ | characteristic thermal time |
| $\rho$ | density of particle | $\theta$ | nondimensional temperature |
| $\tau$ | nondimensional time | | |

## REFERENCES


1. Hwang, C. C. and Pillay, S., "Ignition Delay of Coal Particles in Shock Heated Air," *Comb. Sci. and Tech., 18*:241 (1978).
2. Anderson, W. H. and Gillespie, F. L., "Surface Ignition of Explosives and Propellants by a Hot Stagnant Gas Pocket," *Comb. Sci. and Tech., 24*:35 (1980).
3. Boiko, V. M., Fedorov, A. V., Fomin, V. M., Papyrin, A. N. and Soloukhin, R. I., "Ignition of Small Particles behind Shock Waves," *Progress in Astronautics and Aeronautics, 87*, AIAA, New York, 1981, p. 71.
4. Sichel, M., Baek, S. W., Kauffman, C. W., Maker, B., Nicholls, J. A. and Wolanski, P., "The Shock Wave Ignition of Dusts," *AIAA J., 23*:1374 (1985).
5. Baek, S. W., Sichel, M., Kauffman, C. W., Maker, B., Nicholls, J. A. and Wolanski, P., "The Shock Wave Ignition of Dusts," Poster Session in 20th International Symposium on Combustion," Ann Arbor, MI, 1985.
6. Baek, S. W. and Kauffman, C. W., "On Ignition of Dust Particles in Hot Stagnant Oxygen Gas," *Comb. Sci. and Tech., 56*:149 (1987).

7. Brupbacher, J. M., McCall, M. T. and McCarty, Jr., M., "Shock Tube Combustion of High Density Hydrocarbon Fuels," *Comb. Sci. and Tech., 18*:183 (1978).
8. Seeker, W. R., Wegener, D. C., Lester, T. W. and Merklin, J. F., "Single Pulse Shock Tube Studies of Pulverized Coal Ignition," *Seventeenth Symposium (International) on Combustion*, the Combustion Institute, 1979, p. 155.
9. Davis, W. P., Baer, A. D. and Ryan, N. W., "A Shock Tube Ignition Study of Utah Coal," *Comb. and Flame, 58*:201 (1984).
10. Nettleton, M. A. and Stirling, R., "The Ignition of Clouds of Particles in Shock Heated Oxygen," *Proc. Roy. Soc. London, 300*:62 (1967).
11. Ural, E. A., "Shock Wave Ignition of Pulverized Coal," Ph.D. Thesis, The University of Michigan, 1981.
12. Kauffman, C. W., Wolanski, P., Ural, E., Nicholls, J. A. and Vandyk, R., "Shock Wave Initiated Combustion of Grain Dust," Proceedings of the International Symposium on Grain Dust, Manhattan, Kansas, 1979.
13. Anthony, D. B. and Howard, J. B., "Coal Devolatilization and Hydrogasification," *AlChE J., 22*:625 (1976).
14. Field, M. A., Gill, D. W., Morgan, B. B. and Hawksley, P. G. W., *Combustion of Pulverized Coal*, The British Coal Utilization Research Association, Leatherhead, 1967, p. 329.
15. Borisov, A. A., Gelfand, B. E., Timofeev, E. I., Tsyganov, S. A. and Khomik, S. V., "Ignition of Dust Suspensions behind Shock Waves," Interim Report, Institute of Chemical Physics, USSR Academy of Sciences, Moscow.
16. Merzhanov, A. G. and Averson, A. E., "The Present State of the Thermal Ignition Theory; An Invited Review," *Comb. and Flame, 16*:89 (1971).
17. Bradley, Jr., H. H., "Theory of Ignition of a Reactive Solid by Constant Energy Flux," *Comb. Sci. and Tech., 2*:11 (1970).
18. Liñán, A. and Williams, F. A., "Theory of Ignition of a Reactive Solid by Constant Energy Flux," *Comb. Sci. and Tech., 3*:91 (1971).
19. Liñán, A. and Williams, F. A., "Radiant Ignition of a Reactive Solid with In-Depth Absorption," *Comb. and Flame, 18*:85 (1972).
20. Niioka, T. and Williams, F. A., "Ignition of a Reactive Solid in a Hot Stagnation Point Flow," *Comb. Sci. and Tech., 29*:43 (1977).
21. Liñán, A. and Crespo, A., "An Asymptotic Analysis of Radiant and Hypergolic Ignition of Solid Propellant," *Comb. Sci. and Tech., 6*:223 (1972).
22. Kindelan, M. and Liñán, A., "Gasification Effects in the Heterogeneous Ignition of a Condensed Fuel by a Hot Gas," AFOSR Technical Report 73-2535, European Office of Aerospace Research and Development, 1976.
23. Bradley, Jr., H. H. and Williams, F. A., "Theory of Radiant and Hypergolic Ignition of Solid Propellants," *Comb. Sci. and Tech., 2*:41 (1970).
24. Niioka, T., "Heterogeneous Ignition of a Solid Fuel in a Hot Stagnation Point Flow," *Comb. Sci. and Tech., 18*:207 (1978).
25. Waldman, C. H., "Theory of Heterogeneous Ignition," *Comb. Sci. and Tech., 2*:81 (1970).
26. Kinderlan, M. and Williams, F. A., "Radiant Ignition of a Combustible Solid with Gas Phase Exothermicity," *Acta Astronautica 2*:955 (1976).
27. Kinderlan, M. and Williams, F. A., "Gas Phase Ignition of a Solid with In Depth Absorption of Radiation," *Comb. Sci. and Tech., 16*:47 (1977).
28. Poland, J., Hindash, I. O. and Kassoy, D. R., "Ignition Processes in Confined Thermal Explosions," *Comb. Sci. and Tech., 27*:215 (1982).
29. Waldman, C. H. and Summerfield, M., "Theory of Propellant Ignition by Heterogeneous Reaction," *AIAA J., 7*:1359 (1969).
30. Williams, F. A., "Theory of Propellant Ignition by Heterogeneous Reaction," *AIAA J., 4*:1354 (1966).

31. Annamalai, K. and Durbetaki, P., "A Theory on Transition of Ignition Phase of Coal Particles," *Comb. and Flame, 29*:193 (1977).
32. Liñán, A., "Theory of Heterogeneous Ignition under Convective Heating," AFOSR Technical Report 73-2535, European Office of Aerospace Research and Development, 1976.
33. Henderson, C. B., "Drag Coefficient of Spheres in Continuum and Rarefied Flows," *AIAA J., 14*:707 (1976).
34. Fox, T. W., Rackett, C. W. and Nicholls, J. A., "Shock Wave Ignition of Magnesium Powders," *Proc. 11th International Symposium on Shock Tubes and Waves*, University of Washington, 1977.
35. Leish, S. O., "Smoldering Combustion in Horizontal Dust Layers," Ph.D. Thesis, The University of Michigan, 1983.
36. Martin, C. R., "Characterization of Grain Dust Properties," Am. Soc. of Agricultural Engineers Summer Meeting, Paper No. 78-3020, Logan, Utah, 1978.
37. Gubin, S. A. and Sichel, M., "Calculation of the Detonation Velocity of a Mixture of Liquid Fuel Droplets and a Gaseous Oxidizer," *Comb. Sci. and Tech., 17*:109 (1977).
38. Oran, E. S., Boris, J. P., Young, T., Flanigan, M., Burks, T. and Picone, M., "Numerical Simulations of Detonations in Hydrogen-Air, and Methane-Air Mixtures," *Eighteenth Symposium (International) on Combustion*, the Combustion Institute, 1981, p. 1641.
39. Baek, S. W., Sichel, M. and Kauffman, C. W., "Asymptotic Analysis of the Shock Wave Ignition of Dust Particles," To appear in *Comb. and Flame*.
40. Baek, S. W., "The Ignition of Dust Particles behind Moving Shock Waves," Ph.D. Thesis, The University of Michigan, 1985.
41. Prins, W., Siemons, R., Van Swaaij, W. P. M. and Radovanovic, M., "Devolatilization and Ignition of Coal Particles in a Two-Dimensional Fluidized Bed," *Comb. and Flame, 75*:57 (1989).
42. Ding-Guo, X. and Libby, P. A., "The Burning of Graphite Spheres with Gas-Phase Equilibrium," *Comb. and Flame, 67*:37 (1987).